ResearchGate

See discussions, stats, and author profiles for this publication at: https://www.researchgate.net/publication/222658278

A Review of Conduction Phenomena in Li-Ion Batteries

Article *in* Journal of Power Sources · December 2010

DOI: 10.1016/j.jpowsour.2010.06.060

CITATIONS
586

READS
1,143

5 authors, including:

Myounggu Park
SK innovation, ROK
16 PUBLICATIONS **1,072** CITATIONS
SEE PROFILE

Greg Less
University of Michigan
10 PUBLICATIONS **667** CITATIONS
SEE PROFILE

Ann M Sastry
Sakti3
129 PUBLICATIONS **4,881** CITATIONS
SEE PROFILE

All content following this page was uploaded by Myounggu Park on 23 June 2018.

The user has requested enhancement of the downloaded file.

Journal of Power Sources xxx (2010) xxx–xxx

Contents lists available at ScienceDirect

Journal of Power Sources

journal homepage: www.elsevier.com/locate/jpowsour

Review

A review of conduction phenomena in Li-ion batteries

Myounggu Park[a], Xiangchun Zhang[a], Myoungdo Chung[a], Gregory B. Less[a], Ann Marie Sastry[a,b,c,*]

[a] Department of Mechanical Engineering, University of Michigan, Ann Arbor, MI 48109, United States
[b] Department of Material Science and Engineering, University of Michigan, Ann Arbor, MI 48109, United States
[c] Department of Biomedical Engineering, University of Michigan, Ann Arbor, MI 48109, United States

ARTICLE INFO

Article history:
Received 12 May 2010
Received in revised form 16 June 2010
Accepted 17 June 2010
Available online xxx

Keywords:
Ionic conduction
Electrical conduction
Cathode
Anode
Electrolyte
Lithium-ion battery

ABSTRACT

Conduction has been one of the main barriers to further improvements in Li-ion batteries and is expected to remain so for the foreseeable future. In an effort to gain a better understanding of the conduction phenomena in Li-ion batteries and enable breakthrough technologies, a comprehensive survey of conduction phenomena in all components of a Li-ion cell incorporating theoretical, experimental, and simulation studies, is presented here. Included are a survey of the fundamentals of electrical and ionic conduction theories; a survey of the critical results, issues and challenges with respect to ionic and electronic conduction in the cathode, anode and electrolyte; a review of the relationship between electrical and ionic conduction for three cathode materials: $LiCoO_2$, $LiMn_2O_4$, $LiFePO_4$; a discussion of phase change in graphitic anodes and how it relates to diffusivity and conductivity; and the key conduction issues with organic liquid, solid-state and ionic liquid electrolytes.

© 2010 Published by Elsevier B.V.

Contents

* Corresponding author at: Department of Mechanical Engineering, University of Michigan, Ann Arbor, MI 48109, United States.
Tel.: +1 734 998 0006; fax: +1 734 998 00283.
E-mail address: amsastry@umich.edu (A.M. Sastry).

0378-7753/$ – see front matter © 2010 Published by Elsevier B.V.
doi:10.1016/j.jpowsour.2010.06.060

Please cite this article in press as: M. Park, et al., J. Power Sources (2010), doi:10.1016/j.jpowsour.2010.06.060

Nomenclature

Physical constants

e	charge of an electron, 1.602×10^{-19} C
F	Faraday's constant, 96,487 C mol^{-1}
$\hbar$	reduced Planck's constant, 1.055×10^{-34} J s
k_B	Boltzmann constant, 1.38054×10^{-23} J K^{-1}
m	mass of an electron, 9.11×10^{-31} kg
N_A	Avogadro's number, 6.0232×10^{23} g^{-1} mol^{-1}
R_g	universal gas constant, 8.3141 J mol^{-1} K^{-1}

Symbols

a	inter-atomic distance, m
$\bar{c}$	average concentration, mol L^{-1}
c_A	concentration of species A, mol cm^3
c_B	concentration of species B, mol cm^3
$c_{A,\infty}$	uniform concentration of species A after relaxation, mol cm^3
$c_{B,\infty}$	uniform concentration of species B after relaxation, mol cm^3
$c_{i,j}$	concentration of i in phase j, mol cm^3
$\hat{C}_P$	volume averaged heat capacity at constant pressure, J kg^{-1} °C^{-1}
$\hat{C}_{Pa}$	heat capacity at constant pressure, J g^{-1} K^{-1}
$\hat{C}_{Pi,j}$	partial molar constant pressure heat capacity of species i in phase j, J mol^{-1} K^{-1}
$C_{p\infty}$	partial molar constant pressure heat capacity after relaxation 1, J mol^{-1} K^{-1}
C_{p1}	partial molar constant pressure heat capacity for reaction 1, J mol^{-1} K^{-1}
D_i	diffusivity of solute i (i = 1, 2), cm^2 s^{-1}
D^o	pre-exponential factor, cm^2 s^{-1}
D_{GB}	grain boundary diffusivity, cm^2 s^{-1}
E	energy of an electron, eV
E_a	activation energy, kJ mol^{-1}
E_F	Fermi energy, eV
E_g	band gap, eV
f	friction coefficient, kg m^{-1}
q_{conv}	heat generation rate due to convection, W m^{-3}
q_i	charge of solute 'i (i = 1,2)', C
$q_{heat,i}$	heat generation rate at node i, W
R	electrical resistance, Ω
R_i	internal resistance of the cell, Ω
R_o	radius of sphere (particle), m
R_s	sheet resistance, Ω cm^2
r	inter-particle distance, m
T	temperature, K
T_i	temperature at node i, K
T_j	temperature at node j, K
t	time, s
$U(r)$	inter-particle potential, eV
u_i	mobility of a solute 'i', m^2 V^{-1} s^{-1}
$U_{1,avg}$	theoretical open-circuit potential for reaction 1 at the average composition relative to a reference electrode of a given kind, V
V	cell potential, V
$\bar{V}_{B,\infty}$	partial molar volume of species B after relaxation, m^3 mol^{-1}
v_f	velocity of electrons at steady state, m s^{-1}
v_i	velocity of a solute 'i', m s^{-1}
v_F	Fermi velocity, cm s^{-1}
y	distance from surface along grain boundary, cm
z_i	valence of ion

Abbreviations

AC	alternating current
CV	cyclic voltammetry
CPR	current pulse relaxation
DC	direct current
DEC	diethyl carbonate
DMC	dimethyl carbonate
EC	ethylene carbonate
ρ	density, k gm^{-3}
ν^o	attempt frequency of the order of Debye frequency of the lattice, s^{-1}
ξ	electric field, V m^{-1}
σ	electronic conductivity, S cm^{-1}
τ	relaxation time (average time between two consecutive collisions), s
f_a	F/R_gT, V^{-1}
G	Gibbs free energy, J
h	Joint thickness of porous electrodes and electrolyte layer, cm
ΔH	enthalpy of reaction, J
$\bar{H}_A$	enthalpy of the system of species A, J
$H^o_{1,m}$	molar enthalpy of species 1 in the secondary reference state corresponding to phase m, J mol^{-1}
I	electrical current or cell current, A
i	operating current, A
I_1	partial current of electrode reaction 1, A
j	current density (electron flux), A m^{-2}
j_i	ionic flux, mol cm^{-2} s^{-1}
k	wave vector, m^{-1}
k_a	thermal conductivity, W cm^{-1} s^{-1} K^{-1}
k_{heat}	thermal conductivity, W cm^{-1} K^{-1}
$k_{heat,x}$	thermal conductivity in x direction, W cm^{-1} K^{-1}
$k_{heat,y}$	thermal conductivity in y direction, W cm^{-1} K^{-1}
$k_{heat,z}$	thermal conductivity in z direction, W cm^{-1} K^{-1}
$k_{heat,ij}$	thermal conductivity between node i and node j
$\tilde{M}_i$	molecular weight (i = 1, 2), u
M_i	heat capacity at node i, J K^{-1}
m_e	effective mass of an electron, kg
m_p	effective mass of a hole, kg
$N(E_F)$	number of electrons at E_F, mol eV^{-1}
N_f	number of electrons at steady state, mol m^{-3}
n_i	number of electrons, cm^{-3}
$n_{i,j}$	moles of species i in phase j, mol
p	pressure in atmosphere, Pa
p_i	number of holes, cm^{-3}
q	heat transfer rate, W
q_{heat}	heat generation rate, W m^{-3}
EIS	electrochemical impedance spectroscopy
ESD	electrostatic spray deposition
EVS	electrochemical voltage spectroscopy
GITT	galvanostatic intermittent titration technique
HOPG	highly oriented pyrrolytic graphite
HTT	heat treatment temperature
MCMB	mesocarbon microbeads
PC	propylene carbonate
PLD	pulsed laser deposition
PITT	potentiostatic intermittent titration technique
PSCA	potential step chronoamperometry
PVdF	polyvinylidene fluoride
RPG	ratio of potentio-charge capacity to galvano-charge capacity

Please cite this article in press as: M. Park, et al., J. Power Sources (2010), doi:10.1016/j.jpowsour.2010.06.060

RT	room temperature, 20 °C
SBR	styrene-butadiene rubber
SEI	solid–electrolyte interphase

Greek symbols

α	constant
β	separation of particles at $W(r) = 0$, m
γ	friction coefficient, kg m^{-1}
$\gamma_{i,j}$	activity coefficient of species i in phase j
δ	width of grain boundary, m
ε	permittivity, F m^{-1}
ε_r	relative permittivity
η	depth of potential well of $W(r)$, eV
Λ	dimensionless Ohmic potential drop
μ	viscosity, kg m^{-1} s^{-1}
μ_i	chemical potential of solute 'i', J mol^{-1}
μ_e	electron mobility, m^2 V^{-1} s^{-1}
μ_h	hole mobility, m^2 V^{-1} s^{-1}

1. Introduction

Improvements in the capacity of modern lithium (Li) batteries continue to be made possible by enhanced electronic conductivities and ionic diffusivities in anode and cathode materials. Fundamentally, such improvements present a materials science and manufacturing challenge: cathodes in these battery cells are normally comprised of metal oxides of relatively low electronic conductivity, and separator/electrolyte compositions must be tuned to readily admit ions, while simultaneously forming safe, impenetrable and electronically insulating barriers. The challenges faced by researchers in this field include the relatively low electrical and ionic conductivity values in cells, an unclear relationship between electrical conduction and ionic conductivity in cathode materials, constantly changing conduction properties in anode materials dependent upon phase transformations, and the inherent difficulty in identifying and measuring the microstructure and conductivity of the solid–electrolyte interphase (SEI) film.

Since the Sony Corporation first successfully marketed a commercial Li-ion battery in 1991 [1], Li-ion battery technology has been applied to both thin, light, and flexible portable electronic devices and more recently, to batteries for transportation systems [2] including hybrid and electric vehicles. Though these markets present different challenges in battery cell design, the former requiring in general higher power density, and the latter requiring higher energy density for greater degrees of vehicle electrification, the technical requirements of improved conductivity and diffusivity are common to both.

Models of battery cells and materials [3–5] critically require the best available estimates for conductivity and diffusivity, in order to both predict response and design improved materials. Models at the atomistic and molecular [6–9], particle, both for solids of revolution [10–16], and for fibers [17–21] and continuum [22–29] scales all contribute to improved understanding of cell response. In order, atomistic and molecular models can be used to identify materials architectures of intrinsically high conductivity/diffusivity; particle-based models can be used to identify/design particle shapes and fractions and loading schema of additives that tune conductivity/diffusivity; and continuum models can best be used as reduced-order inputs to optimization and controls models [26,30–34]. Accordingly, at each scale accurate, validated conductivity/diffusivity values are needed.

Experimental validation of such parameters is often challenging, however. Often, battery materials characterization is carried out *ex situ* or as a *post mortem* analysis because of the complexity of *in situ* experimental setup; though such data is still invaluable for interpreting results, they can only describe the end state. A key challenge remains to develop experimental techniques to probe and detect Li-ion movement within the electrode lattice structure and the electrode–electrolyte interface at a local level as a function of time. Interpretation of *in situ* characterization experiments is challenging often due to a lack of viable theories concerning cathodes, anodes, and novel electrolytes.

While some authors [35,36] have discussed manipulating the electrical and/or ionic conductivity of relevant materials in Li-ion cells, few review papers are dedicated to conduction; papers that do focus on conduction usually discuss only one kind of material (e.g., cathode or anode) or only summarize current key issues, namely: a review of the diffusion problem with respect to ionic conduction [37] in nanocrystalline ceramics with a focus on Nuclear Magnetic Resonance (NMR) spectroscopy, a review of the importance of electrical conduction in cathode materials [38], as well as other more generalized discussions of the conduction problem [39,40]. Thus, a comprehensive survey of conduction phenomena is provided here, for all components of a Li-ion cell, incorporating theoretical, experimental, and simulation studies. Our objectives in this work are to

(1) survey the fundamentals of electrical and ionic conduction theories;
(2) survey the critical results, issues and challenges with respect to electrical and ionic conduction in all of the major battery components including cathode, anode and electrolyte;
(3) review the relationship between electrical and ionic conduction for three cathode materials: $LiCoO_2$, $LiMn_2O_4$, $LiFePO_4$;
(4) review phase change in graphitic anodes and how it relates to diffusivity and conductivity;
(5) review key conduction issues with organic liquid, solid state and ionic liquid electrolytes.

While an attempt has been made to present a unified viewpoint, information has been drawn from many different sources and certain ambiguities and disjointedness are unavoidable. References over 50 years old represent the foundational papers upon which subsequent literature has built and thus are included here.

Finally, although units in the various equations may describe the same physical quantities, they vary with context and therefore have not been standardized. Instead they are maintained as described in the original papers.

2. Review of the fundamentals of conduction

In this section, we introduce the fundamentals of conduction phenomena – ionic and electronic conduction. Based upon this succinct but essential survey, we made careful observations on research efforts in Li-ion batteries, which are discussed in the latter part of this review. Note that this is fundamental physics which has been used many times in research papers dealing with conduction phenomena, first-principle calculations and simulation, as well as experimental papers.

2.1. Conduction in an electrochemical cell

Generally, when working with electrochemical cells (the most basic unit comprising any battery), Li-ion cells included, all key phenomena involve conducting charged particles (electrons and ions) from cathode to anode (primary cell) or vice versa (secondary cell). An operating galvanic cell [41,42] is depicted in Fig. 1 (adapted from [41,42]). Note that in the *redox* reaction shown, two electrons

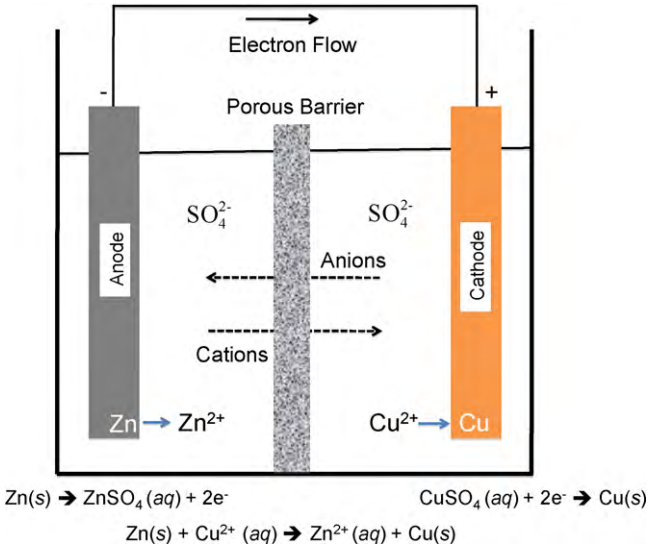

Fig. 1. Generic operating electrochemical cell (adapted from [41,42]).

are transferred. Because the electrochemical reaction of a cell is based upon a change of oxidation state, the ease of electron-transfer between anode and cathode can dictate the magnitude of the cell's driving force [43,44]. Electrons are transferred from anode to cathode during the discharge of a cell; the related cell components are electrodes, current collectors and electrical leads. In addition to electrical conduction, ionic conduction through the electrodes and electrolyte is necessary to complete the electrochemical reaction. For a simple illustration of conduction phenomena, the potential equation of an operating electrochemical cell is surveyed. Generally, the operating voltage (E) of the cell is lower than the standard cell voltage (E_o) due to potential drops caused by several factors. This is stated mathematically [41] as

$$E = E_o - [(\eta_{ct})_a + (\eta_{ct})_c] - [(\eta_c)_a + (\eta_c)_c] - iR_i = iR \qquad (2.1.1)$$

where E_o is the standard cell potential, $(\eta_{ct})_a$, $(\eta_{ct})_c$ are activation polarizations (charge-transfer over voltage) at the anode and cathode $(\eta_c)_a$, $(\eta_c)_c$ are concentration polarizations at the anode and cathode, i is the cell operating current, R_i is the internal resistance of the cell and R is the apparent cell resistance.

All terms in Eq. (2.1.1) can be related to conduction phenomena. Activation and concentration polarizations are connected to the kinetics of charge transfer and mass transfer [44–46], respectively. Internal resistance (R_i) is affected by the conduction properties of various materials and their interfaces and can be broken down as listed in Table 1 [41]; the sum of each of the internal resistances is the total internal resistance. Examining the sources of resistance can provide insight into the key barriers to optimized conduction in electrochemical cells. Given the number of potential sources of resistance in a cell, even the relatively simple phenomenon of potential drop can be quite challenging to interpret quantitatively.

Table 1
Internal resistance of cell [41].

Type of resistance	Internal resistance of cell (R_i = ionic resistance + electrical resistance + interfacial resistance)
Ionic	• Electrode (cathode and anode) particle • Electrolyte
Electrical	• Electrode (cathode and anode) particle • Conductive additives • Percolation network of additives in electrode • Current collectors • Electrical taps
Interfacial	• Between electrolyte and electrodes • Between electrode particles and conductive additives • Between electrode and current collector • Between conductive additives and current collector

2.2. Ionic conduction

2.2.1. Diffusion in condensed materials

Diffusion properties of Li-ion cell determine some of the key performance metrics of Li-ion battery cells, including the charge and discharge rate, practical capacity and cycling stability. The governing equation describing the diffusion process is known as Fick's law (Eq. 1 in Table 2 [47,48]); the proportionality factor D is the diffusivity or diffusion coefficient (Eq. 3–5 in Table 2). In condensed materials (liquids and solids), diffusion is governed by random jumps of atoms or ions, leading to position exchange with their neighbors. The kinetics of this process is temperature dependent and follows an Arrhenius type relationship [49] (Eq. 2 in Table 2). In liquids, the temperature dependence of the diffusion is much less than in solids. Note that no successful first-principles calculation has been made, due to insufficient understanding of the liquid structure [47]. Thus, a simple expression derived from Stoke's drag law [50] is frequently used as an alternative for a diffusivity expression in liquids (Eq. 3 in Table 2) [47,51].

The generic diffusion mechanism for a solid is a good starting point for understanding diffusion processes because diffusivity is highly dependent upon the relevant diffusion mechanism (Table 3) [52]. Defects play the central role and affect the terms – H^F and D^o in Eq. 6 in Table 2. Diffusion mechanisms for solids can be classified into two categories: vacancy/defect-mediated mechanisms, and non-vacancy/non-defect-mediated mechanisms. Vacancy-mediated mechanisms require much larger activation energies than non-defect-mediated mechanisms (Eq. 4 vs. Eq. 5 in Table 2). Similarly, there are two primary defects affecting ion diffusion in ionic crystals – Schottky pairs (cation vacancy plus anion vacancy) and Frenkel pairs (cation vacancy plus a cation intersti-

Table 2
Governing equation for diffusion and diffusion coefficients [47,48].

No.	Title	Equation	Comments
1	Fick's law	$j_i = -D_i \nabla c_i$ & $\frac{\partial c_i}{\partial t} = \nabla \cdot (D \nabla c_i)$	Governing equation for diffusion
2	Arrhenius equation	$rate \approx \exp\left(-\frac{\Delta G}{k_B T}\right)$	Predicts kinetics based on thermal activation
3	Diffusivity in liquid	$D_i = \frac{k_B T}{6\pi\mu R_o}$	Einstein-Stokes relation
4	Diffusivity in solid	$D_i = a_l^2 \Gamma$: a_l is the jump length, $\Gamma = \nu^o \exp\left(-\frac{\Delta G}{k_B T}\right)$	
5	Temperature dependence of diffusivity in solid	$D_i = D^o \exp\left(-\frac{H^M}{k_B T}\right)$	Describes non-defect mediated interstitial diffusion
6	Temperature dependence of diffusivity in solid	$D_i = D^o \exp\left(-\frac{H^F + H^M}{k_B T}\right)$	Describes vacancy mediated diffusion

Please cite this article in press as: M. Park, et al., J. Power Sources (2010), doi:10.1016/j.jpowsour.2010.06.060

Table 3
Diffusion mechanisms in solid [52].

Mechanism		Description
Vacancy (defect)-mediated	Vacancy	Self-diffusion in metals and substitution alloys
	Divacancy	Diffusion via aggregates of vacancies
Non-vacancy (defect)-mediated	Interstitial	Solute atoms considerably smaller than the host atoms, and atoms are incorporated into interstitial sites of the host lattice to form an interstitial solid solution
	Collective	Solute atoms similar in size to host atoms involving simultaneous motion of several atoms. Usually substitutional solid solutions are formed
	Interstitialcy	A collective mechanism important for radiation-induced diffusion. At least two atoms move simultaneously; however, this mechanism is negligible for thermal diffusion
	Interstitial-substitutional Exchange	Solute atoms are dissolved on both interstitial and substitutional sites and diffuse via interstitial or substitutional exchange mechanisms

Table 4
Bonding potentials in Li-ion battery [60–62].

Cell component	Bond type	Interaction potential	Bond length (Å)	Bond strength (kJ mol^{-1})
Anode (graphite, in-plane)	Covalent	–	1.46	374
Anode (graphite, inter-plane)	van der Waals	Lennard-Jones potential $U(r) = 4\varepsilon\left\{\left(\frac{\beta}{r}\right)^{12} - \left(\frac{\beta}{r}\right)^{6}\right\} \cdots (1)$	3.35	5.9
Cathode (spinel, $LiMn_2O_4$)	Ionic	Coulombic interaction $U(r) = \frac{q_1 q_2}{4\pi\varepsilon_r r} \cdots (2)$	1.960 (Li–O)	426.48 (Li–O)
Liquid electrolyte	Coulombic	Coulombic interaction $U(r) = \frac{q_1 q_2}{4\pi\varepsilon_r r} \cdots (3)$	–	–

tial) [53,54]. Ionic solids with Schottky defects (corresponding to the defect-mediated diffusion in Table 3) have lower ionic conductivities and higher activation enthalpies because ionic transport occurs from the motion of vacancies. On the other hand, ionic crystals with Frenkel disorder (corresponding to the interstitial mechanism in Table 3) show higher ionic conductivities and lower activation enthalpies because ionic transport occurs primarily from the motion of interstitial species. Li-ions diffuse mainly by an interstitial mechanism due to their small radius. Although the Li-ion is one of the smallest ions, it is still quite big when compared to electrons; the radius of a Li-ion is ten orders of magnitude larger than that of an electron (radius of a Li-ion: 59×10^{-12} m [55]; radius of an electron: 10^{-22} m [56]). Also the motion of Li-ions is strongly impeded by the potential created by the presence of neighboring ions as discussed below. Thus diffusion can be the rate-determining process compared to electronic conduction in an electrochemical reaction.

In crystalline solids, the structure is well defined and diffusivity can be modeled with a first-principles calculation [57] (Eq. 4 in Table 2). Diffusion in a crystal is strongly affected by bonding potential and defects; the effects are incorporated in the diffusivity expression as enthalpy (H) and a prefactor, D^o (Eqs. 5 and 6 in Table 2) [58,59]. Bond types and potentials of materials used in Li-ion batteries are summarized in Table 4 [60–62]. The two strongest chemical bonds are ionic and covalent; electron-transfer between two species creates ionic bonds, and covalent bonds are formed by electron sharing among atoms. The van der Waals interaction, expressed as the Lennard–Jones potential, is relatively weak despite showing a longer interaction range. In the case of the graphite anode, a Li-ion can easily diffuse parallel rather than perpendicular to the graphene layers during intercalation. Thus in order to understand the diffusion of the Li-ion it is important to consider crystal structure as well as the surrounding potential.

Table 5
Relation between diffusivity and ionic conductivity [51].

No.	Title	Equation	Comments
1	Drift velocity	$v_i = -u_i(\nabla\mu_i + z_i F\nabla\varphi) : \nabla\varphi = \xi$	Drift velocity expressed using mobility and the chemical and electrical potentials
2	–	$\nabla\mu_i = \frac{RT}{c_i}\nabla c_i$	Relationship between and in the dilute case
3	Drift velocity	$-v_i = \frac{u_i RT}{c_i}\left(\nabla c_i + c_i z_i \frac{F\nabla\varphi}{RT}\right)$	Drift velocity in the dilute case
4	Ionic flux	$-j_i = -c_i v_i = u_i RT\left(\nabla c_i + c_i z_i \frac{F\nabla\varphi}{RT}\right) = D_{io}\left(\nabla c_i + c_i z_i \frac{F\nabla\varphi}{RT}\right)$	Definition of ionic flux is combined with Eq. (3)
5	Nernst–Planck relationship	$D_{io} = u_i RT;\ D_i = \frac{D_{io}}{N_A} = \frac{u_i RT}{N_A} = u_i k_B T = \frac{v_i}{\xi} k_B T$	Describes the diffusivity and mobility relationship
6	Current density	$j = q_i j_i = \frac{q_i^2 c_i D_i}{k_B T}\xi = \sigma\xi$	Definition of current density (j), ionic flux (j_i)
7	Diffusivity vs. ionic conductivity	$\sigma = \frac{q_i^2 c_i}{k_B T} D_i$	A generic relationship between diffusivity and ionic conductivity is obtained

Please cite this article in press as: M. Park, et al., J. Power Sources (2010), doi:10.1016/j.jpowsour.2010.06.060

2.2.2. Relationship between diffusivity and ionic conductivity

Although diffusivity is used as a main descriptor for the motion of Li-ions it is indispensible to survey the concept of ionic conduction and the relationship between diffusivity and ionic conductivity because ionic conductivity also is important for describing the motion of Li-ions. Motion of a Li-ion gives rise to ionic conduction (i.e. currents) under external electrical potential. In a Li-ion battery, Li-ions should move through the electrolyte from the cathode to the anode during charge, and vice versa during discharge; anything hampering this motion can be interpreted as ionic resistivity. As shown in Table 1, resistance can originate from inside the electrode materials, from the interface between the electrodes and the electrolyte, and from the electrolyte itself.

Charged particles, including Li-ions, can pass through a media under two driving forces: an externally applied electric field or a concentration gradient. The mobility (u_i) of ions represents the degree of ease with which ions pass through media when an external electrical field is applied, and the diffusivity (D_i) represents the ease with which ions pass through media under a concentration gradient. While mobility and diffusivity are often treated as separate phenomena, Table 5 summarizes the key equations for deriving the relationship between them (and then for ionic conductivity) as previously described [51]. Indeed, it can be shown that mobility and diffusivity are the same physical entity [51]. The key here is that diffusivity, mobility, and ionic conductivity are related properties. Derivations of the relationships follow.

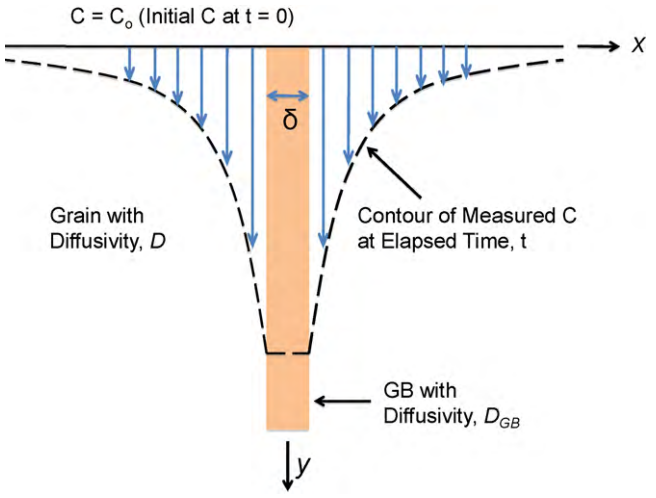

Fig. 2. GB diffusion model by Fisher (adapted from [67–69]).

The relationship between mobility and diffusivity can be obtained by considering the drift velocity (v_i) of ions in terms of mobility (u_i) under both an externally applied electric field and a concentration gradient (Eqs. 1–5 in Table 5). The Nernst–Planck equation (Eq. 5 in Table 5) implies that mobility and diffusivity are interchangeable. Using the definition of current density induced by

Table 6
Grain Boundary Diffusivity [67,68,70].

No.	Title	Equation	Comments
1-1	Fisher's model	$\left(\frac{\partial \ln \bar{c}}{\partial y}\right)^2 = \frac{1}{D_{GB}\delta}\left(\frac{4D_i}{t}\right)^{1/2}\pi^{-1/2}$	• Approximate solution easily applied to experimental results • A plot of log $\bar{c}$ vs. y yields a straight line with slope given in Eq. (1-1)
1-2		$D_{GB}\delta = \left(\frac{\partial \ln \bar{c}}{\partial y}\right)^{-2}\left(\frac{4D_i}{t}\right)^{1/2}\pi^{-1/2}$	• Rearranging Eq. (1-1), we can get D_{GB}
2-1	Whipple's model	$\left(\frac{\partial \ln \bar{c}}{\partial y^{6/5}}\right)^{5/3} = \frac{1}{D_{GB}\delta}\left(\frac{4D_i}{t}\right)^{1/2}(0.78)^{5/3}$	• Exact solution but inconvenient to apply for experimental results • A plot of log $\bar{c}$ vs. $y^{6/5}$ yields a straight line with slope given in Eq. (1-1)
2-2		$D_{GB}\delta = \left(\frac{\partial \ln \bar{c}}{\partial y^{6/5}}\right)^{-5/3}\left(\frac{4D_i}{t}\right)^{1/2}(0.78)^{5/3}$	• Rearranging Eq. (2-1), we can get D_{GB}

Table 7
Room temperature resistivity for various materials.

Cell Component	Material	Band gap (eV)	Electrical conductivity (S cm^{-1})	Reference
Current collector (anode)	Copper (C11000)	0	5.8×10^5	[75,76]
Current collector (cathode)	Aluminum (1100)	0	3.4×10^5	[75,77]
Anode	Graphite	0	$(2–1) \times 10^3$	[78–80]
Cathode	$LiCoO_2$	0.5–2.7	$\sim 10^{-4}$	[81–83]
	$LiMn_2O_4$	0.28–2.2	$\sim 10^{-6}$	[84–90]
	$LiFePO_4$	0.3–1	$\sim 10^{-9}$	[91,92]

Table 8
Equations related to classical concept of electrical conductivity [94].

No.	Title	Equation	Comments
1	Electron gas force equilibrium equation	$m\frac{dv}{dt} + \gamma v = e\xi$	Electrons moving in a solid can be modeled as a flowing gas experiencing friction
2	Velocity of electron gas	$v = v_f\left[1 - \exp\left(-\left(\frac{e\xi}{mv_f}t\right)\right)\right]$; $v_f = \frac{\tau e\xi}{m}$	Steady state solution to Eq. (1)
3	Steady state current density	$j = N_f v_f e = \sigma\xi$	Eq. (3) can be derived from Ohm's law
4	Conductivity	$\sigma = \frac{N_f e^2 \tau}{m}$	

Please cite this article in press as: M. Park, et al., J. Power Sources (2010), doi:10.1016/j.jpowsour.2010.06.060

Table 9
Equations related to electrical conductivity modified by quantum mechanics [94,95,74].

No.	Title	Equation	Comments
1	Current density	$j = v_F eN(E_F)\Delta E = v_F eN(E_F)\frac{dE}{dk}\Delta k$	Expression modifying Eq. (3) in Table 3 to consider the electrons near the Fermi level
2	Current density	$j = \frac{1}{3}v_F^2 e^2 N(E_F)\tau E = \sigma E$	Simplification of Eq. (1)
3	Conductivity	$\sigma = \frac{1}{3}e^2 v_F^2 \tau N(E_F)$	Expression for conductivity of conductor derived from Ohm's law
4	Conductivity	$\sigma = (n_i e\mu_e + p_i e\mu_h)$	Expression for conductivity of an intrinsic semiconductor considering both electrons and holes (for details see ref. [74])
5	Concentration of charge carriers	$n_i = p_i = 2\left(\frac{k_B T}{2\pi\hbar^2}\right)^{3/2}(m_e m_h)^{3/4}\exp\left(-\frac{E_g}{2k_B T}\right)$	Expression for charge carrier concentration in the band gap (for details see ref. [74])

ionic flux (Eq. 6 in Table 5), along with either Eq. 4 or 5 in Table 2, the relationship between diffusivity and ionic conductivity is easily obtained (Eq. 7 in Table 5). Consequently, if the contribution of ionic conduction to the total conduction [63] (electrical conduction + ionic conduction) is known, diffusivity can then be deduced, [64] and vice versa. Generally, diffusivity in electrode materials is hard to measure experimentally. Ionic conductivity, however, is relatively easy to measure and as has been shown diffusivity and mobility (or ionic conductivity) can be interconverted and complement each other. Thus, diffusivity can be deduced from measuring ionic conductivity. Note that most often adopted diffusivity measurement techniques including CV, GITT, PITT and EIS measure the variation of ionic current under applied voltage to calculate diffusivity.

2.2.3. Grain boundary diffusion

To fully understand diffusion phenomena and obtain realistic diffusivity values for electrode materials, the effects of the micro- and macro-structure as well as grain boundaries should be taken into account. The grain boundary (GB) is defined as the interface between two crystals (or grains). The GB differs from the grains in either crystallographic orientation, composition, bonding state or crystal lattice dimensions [65]. The features of GB diffusion are low migration barriers (H^M and/or H^F in Eqs. 5 and 6 in Table 2) and a high concentration of diffusion-mediating defects due to incomplete bonding or disorder; thus, the diffusivity value along a GB is higher than that within grains [66]. First-principles techniques are hard to apply to GB structures due to disorder, and therefore a continuum model that considers grain boundaries as slabs is usually adopted to analyze grain boundary diffusion (Fig. 2 adapted from [67–69]). Two frequently used continuum model solutions for GB diffusion [67,70] are shown in Table 6 [67,68,70]. Both models have been analyzed [71] in terms of solution form: Fisher's Model described in [67],is an approximate solution easily applied to experimental results, whereas Whipple's Model described in [70] is an exact solution that is inconvenient to apply due to its integral form. Fig. 2 shows the general trend of isoconcentration line (Fisher's solution) change as a function of time using the model derived in [67]. As expected, along the grain boundary solute atoms diffuse much faster. For example it is reported that the ratio of D_{GB}/D_i is about 10^{10} at 200 °C for Ag [68].

2.3. Electrical conduction

2.3.1. Electrical conductivity

The differences in electrical properties of materials, e.g., insulators, semiconductors and conductors, originate from the band structures described by quantum mechanics [72–74]. An insulator usually has a completely filled valence band and an empty conduction band with a large band gap, while conductors have a partially filled valence band (metal) or overlapped bands (semimetal), thus helping electrons in the crystal move easily when an external electrical field is applied. The band gap and conductivity at room temperature (RT) of various materials used for Li-ion batteries is summarized in Table 7 ([75–92]). Metallic materials (band gap = 0) have very high electrical conductivities, and electron transport is the dominant conduction mechanism. Graphite shows highly anisotropic electrical conduction properties [93] as shown by the theoretically calculated values given in Table 19. For materials having a non-zero band gap low conductivity is usual, and overall conduction can be considered as the summation of ion and electron transport. This makes ionic conduction more important for semiconductors and insulators than for electrically conductive materials. However, there are no viable theories yet developed to quantitatively describe conduction properties using band gap analysis. Therefore, the usual approach relies upon the classical concept of conductivity to describe conducting materials such as a metal. This classical concept will be briefly introduced here along with an advanced concept of conductivity based on quantum mechanics [94,95].

From the classical point of view, electrical conduction is considered to be the flow of a free electron gas. When a free electron gas flows under an externally applied electric field, a friction force (γv) hinders the flow; this friction force can be interpreted as electrical resistance. This force equilibrium is expressed in Eq. 1 in Table 8 [94]. From the steady state solution to force equilibrium, electron

Table 10
Li-ion diffusivity and electrical conductivity of cathode materials.

Cathode material	D_{Li} ($cm^2\ s^{-1}$)	σ ($S\ cm^{-1}$)	Year	Reference
$LiCoO_2$	10^{-10} to 10^{-8}	10^{-4}	2002, 2001, 1996	[97–99]
$LiMn_2O_4$	10^{-11} to 10^{-9}	10^{-6}	2002, 1999, 1996	[85,86,100,101]
$LiFePO_4$	10^{-14} to 10^{-15}	10^{-9}	2004, 2003, 2001	[91,92,102]

Please cite this article in press as: M. Park, et al., J. Power Sources (2010), doi:10.1016/j.jpowsour.2010.06.060

Table 11
Diffusivity of Li-ion in $LiCoO_2$ under various conditions.

Cathode material	Diffusivity ($cm^2\ s^{-1}$)		Description	Measurement technique	Reference
Li_xCoO_2	• 1.5×10^{-10} to 8.0×10^{-8} (single particle)		• 2D layered structure: $R\bar{3}m$ • Diffusion mechanism: divacancy	PSCA	[108,97]
	• 1.0×10^{-11} to 1.0×10^{-7} (single particle)		• 3.85 V < E/V vs. Li/Li^+ < 4.2 V	EIS	
	• 4.0×10^{-11} to 3.0×10^{-10} ($0.45 < x < 0.7$)		• Thin film electrode	PITT	[109]
	• 0.1×10^{-9} to 1.5×10^{-9} ($0.3 < x < 0.85$)		• Single phase region: $0.45 < x < 0.75$ • Two phase region ($0.75 < x < 0.93$)	EVS	[98]
	• 9.0×10^{-13} (particle size: 60 nm)		• Effect of nano-sized particle • At 3.2 V vs. Li/Li^+	EIS	[110]
$Li_{0.5}CoO_2$	(003) • 1.9×10^{-12} (GITT) • 1.6×10^{-13} (PITT) • 1.6×10^{-10} (EIS) • 6.4×10^{-13} (CV)	(104) • 3.2×10^{-11} (GITT) • 1.8×10^{-11} (PITT) • 6.0×10^{-9} (EIS) • 7.7×10^{-12} (CV)	• Thin film electrode • Crystal orientation dependence (003): thin film thickness, 0.31 μm (104): thin film thickness, 1.35 μm	Various	[111]
$Li_aNi_{1-x}Co_xO_2$	• 8×10^{-9} to 2×10^{-8}: (a = 0, 0.7, 0.8, 0.9 and $0.3 < x < 0.8$)		• Diffusivity insensitive to a and x	GITT	[112]
$Li_xCo_{0.5}Ni_{0.5}O_2$	• 9×10^{-12} to 3×10^{-11} ($0.2 < x < 0.9$)		• Investigate diffusion mechanism using D_s and Φ	GITT	[113]
$LiCo_{1-x}Al_xO_2$	• 0.5×10^{-15} to 3.0×10^{-15} ($x = 0$)		• Al doping inhibits anisotropic expansion of structure	EIS	[114]
a-Carbon coated $LiCoO_2$	• 8.0×10^{-15} to0.5×10^{-14} ($x = 0.1$) • 1.21×10^{-10}: bare $LiCoO_2$: • 1.73×10^{-8}: C-coated $LiCoO_2$:		• Amorphous-carbon-coating increased diffusivity	EIS	[115]
$LiFePO_4$ coated $LiCoO_2$	5 cycles • 1.2×10^{-11} (bare) • 1.1×10^{-11} (coated)	50 cycles • 0.38×10^{-11} (bare) • 1.1×10^{-11} (coated)	• 5 wt% $LiFePO_4$ coating • Good diffusivity retention • At 4.05 V vs. Li/Li^+	GITT	[116]

velocity (v_f) can be obtained (Eq. 2 in Table 8), which allows current density (j) to be written as Eq. 3 in Table 8. Finally, an expression for electrical conductivity (σ) (Eq. 4 in Table 8) can be obtained from the expression for current density (j). Thus, electrical conductivity, derived from the classical point of view, implies that the conductivity of a material increases when a large number of free electrons exist and the relaxation time τ, i.e. the average time between collisions, is long. This model has been successfully applied to describe conduction in metallic materials.

The conductivity expression derived via quantum mechanical concepts is more meaningful than that derived from the classical model, because it considers electrons and the density of states near the Fermi level. Quantum mechanical concepts can also help to understand the effects of doping, the intentional introduction of impurities to vary the carrier concentration, as discussed in later sections. From a quantum mechanics point of view, only some electrons (near the Fermi level) displaced due to an electrical field are accelerated, and electron movement is considered only in the direction of the electric field [94]. The interaction potential must also be considered. Displaced free electrons have equal or slightly higher velocities than the Fermi velocity (v_F). The current density can be written as Eq. 1 in Table 9 [74,94,95] where $N(E_F)$ is the electron population indicating available energy densities at the Fermi level. The current density is obtained as shown in Eq. 2 in Table 9 by substituting expressions for dE/dk and Δk into Eq. 1. The expression for electrical conductivity is obtained as in Eq. 3 in Table 9. The resulting conductivity expression can be used to correlate conductivity differences among classes of materials (i.e. conductors, semiconductors or insulators) as well as within the same class of materials. However, expressions for the electrical conductivity of semiconductors are generally more complex due to the band gap and temperature dependence of carrier concentration (Eqs. 4 and 5 in Table 9).

The cathode materials analyzed in this review are semiconductors (Section 3.2) as defined by their band gaps (see Table 7); the band gap of Si, Ge, GaAs (generic semiconductors used in electronics industry) are 1.17, 0.744, 0.43 eV, respectively. A general expression for electrical conductivity of intrinsic semiconductors is shown in Eq. 4 in Table 9. The effects of temperature and band gap on conductivity are contained in Eq. 5 in Table 9

Please cite this article in press as: M. Park, et al., J. Power Sources (2010), doi:10.1016/j.jpowsour.2010.06.060

Table 12
Diffusivity of Li-ion in $LiMn_2O_4$ under various conditions.

Cathode material	Diffusivity ($cm^2\ s^{-1}$)	Description	Measurement technique	Reference
$Li_xMn_2O_4$	• 3.2 to 1.38×10^{-11}: single crystal	• 3D Spinel Structure:, Cubic • E/V vs. Li/Li^+: 3.8, 3.9, 4.08 V	PSC	[117]
	• 0.7×10^{-8} to 3.4×10^{-8}: parent particles	• Oxidative treatment resulted in finer particles: not advantageous	EVS, GITT	[100]
	• 1.0×10^{-10} to 4.0×10^{-9}: oxidative treatment • 6×10^{-11} to 5×10^{-10} (particle: 20 μm)	• $0.08 < x < 0.96$ • Porous laminate vs. ESD thin film electrodes	PITT	[101]
	• 6×10^{-11} to 5×10^{-10} (thickness: 10 μm)	• 4.07 V < E/V vs. Li/Li^+ < 4.19 V		
	• 1.71×10^{-12}: bare sample	• SEI layer effect: thin film (0.5 μm thickness) with nanosized grains (100 nm)	PSCA	[118]
	• 4.67×10^{-13}: sample after 15 cycles • 10^{-10}: highly crystalline film (PLD) • 10^{-8}: oxygen rich defective film (UVPLD)	• Effects of thin film fabrication process	CV	[119]
$LiAl_xMn_{2-x}O_4$	• 2.7×10^{-11} ($x = 0$) • 26×10^{-12} ($x = 0.125$) • 8.0×10^{-12} ($x = 0.25$) • 4.4×10^{-12} ($x = 0.375$)	• Al doping shrinks diffusion path and decrease diffusivity • At 4.05 V vs. Li/Li^+	EIS	[120]
$Li_xB_y\ Mn_{2-y}\ O_4$	• 5.0×10^{-10} to 5.0×10^{-9} ($y = 0$) • 5.0×10^{-9} to 8.0×10^{-9} ($y = 1/6$) • 8.0×10^{-9} to 1.0×10^{-8} ($y = 1/3$)	• B doping increases D_{Li} • Composite electrode • $0.08 < x < 0.96$	CPR	[121]
$Li_yMn_{2-y}O_4$ (M = Co, Cr, Fe, Ni)	• 10^{-9} to 10^{-10} ($y = 0$)	• Doping increase due to weakening Li–O bonding and/or disorder/order in spinel structure	PITT	[122,123]
	• 1×10^{-10} to 5.0×10^{-8} ($y = 1/6$: Co or Cr) • 6.5×10^{-10} to 5.0×10^{-8} ($y = 1/6$: Fe) • 2.3×10^{-11} to 1.8×10^{-8} ($y = 1/6$: Ni)	• $\sim 0.2 < x < \sim 0.85$	GITT	

3. Survey of conduction studies in cathode materials

Since the invention of Li-ion batteries, three cathode materials, $LiCoO_2$, $LiMn_2O_4$ and $LiFePO_4$, have represented the majority of Li-ion cathode research. For illustrative purposes, Fig. 3 depicts conduction phenomena in a single composite cathode particle ($LiFePO_4$ in contact with conductive additive and binder) during charge. When a Li-ion diffuses out of the cathode (ionic conduction) during the charge cycle the valence state of the transition metal ion changes (electronic conduction); the Fe^{2+} ion is oxidized to Fe^{3+}.

Table 13
Diffusivity of Li-ion in $LiFePO_4$ under various conditions.

Cathode material	Diffusivity ($cm^2\ s^{-1}$)	Description	Measurement techniques	Reference
$LiFePO_4$	• 1.6×10^{-9}: [0 0 1], *c* direction at 147 °C • $<10^{-10}$: [100], *a* direction at 146 °C • 2.4×10^{-9}: [0 1 0], *b* direction at 146 °C	• Olivine structure: *Pnma* • Crystal orientation dependence	DC polarization	[124]
$Li_{1-x}FePO_4$	• 4.97×10^{-16} to 9.13×10^{-15} ($0.1 < x < 0.9$) • 1.91×10^{-15} to 1.29×10^{-14} ($0.1 < x < 0.9$)	• Effect of delithiation	GITT EIS	[102]
$LiFe_{1/4}Mn_{1/4}Co_{1/4}Ni_{1/4}PO_4$	• 10^{-15}	• Quaternary solid solution of transition metals	GITT	[125]
$LiFe_{1-x}Mn_xPO_4$	• $\sim 10^{-13}$ to $\sim 10^{-12}$ ($0 < x < 0.2$)	• Mn doping changed crystal structure	CV	[126]
Al-doped $LiFePO_4$	• 6.0×10^{-8}: [001], *c* direction at 180 °C • 1.0×10^{-9}: [1 0 0], *a* direction at 180 °C • 7.0×10^{-8}: [0 1 0], *b* direction at 180 °C	• Crystal orientation dependence • Diffusion preference in b, c plane	DC polarization	[127]
$LiZn_{0.01}Fe_{0.99}PO_4$	• 9.98×10^{-14}: undoped sample • 1.58×10^{-13}: doped sample	• Zn doping increased diffusivity • Pillar effect	EIS	[128]
$Li_{1-x}FePO_4$/C composite	• 2.9×10^{-11} to 1.1×10^{-12} ($0 < x < 1$)	• Effect of nano-size particle (300 nm)	EIS	[129]
C-coated Li_xFePO_4	• 1.27×10^{-16}: $x = 0$ • 8.82×10^{-18}: $x = 0.9$ • 5.95×10^{-17}: 5th cycle • 5.44×10^{-17}: 50th cycle	• Bare sample • $FePO_4$: lower diffusivity • C coated sample • Good diffusivity retention	EIS	[130]

Please cite this article in press as: M. Park, et al., J. Power Sources (2010), doi:10.1016/j.jpowsour.2010.06.060

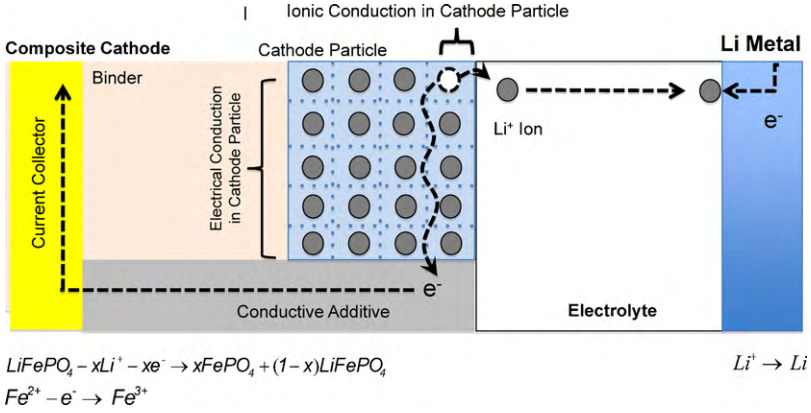

Fig. 3. Conduction phenomena in cathode particle ($LiFePO_4$) during charge.

Thus, it is important that electrical and ionic conductivities be optimized in cathode materials, since either of these values can dictate the overall cell properties including capacity and cycle life [64,96]. However, assuming that diffusion governs charge/discharge rates, greater emphasis usually falls on ionic conductivity rather than electronic conductivity, since high ionic conductivity will allow the rapid diffusion of Li-ions into the cathode material. Average values of Li-ion diffusivity and electrical conductivity for different cathode materials are summarized in Table 10 [85,86,91,92,97–102]. Note that both the Li-ion diffusivity and electrical conductivity of $LiCoO_2$ are superior to those of $LiFePO_4$ and $LiMn_2O_4$, yielding a possible reason that $LiCoO_2$ displays a higher realized percent of theoretical capacity [38] than the other cathode materials. Efforts to manipulate the ionic and electrical conductivity of $LiFePO_4$ and $LiMn_2O_4$ via doping have not yet been rewarding. To date, only conductive coatings and particle size reduction techniques have resulted in higher conductivity for cathode materials.

3.1. Ionic conduction in cathode materials

When discussing ionic conduction in crystals, it is necessary to consider the structure of the host species. Diffusion of a Li-ion in a cathode particle is strongly dependent upon the interaction potential between the Li-ion and the host material structure. In Table 6 interaction potentials are given for the different cell components with representative values for various materials. A simple model for determining the diffusion path of ions in various crystal structures is introduced in [103]. This model describes the diffusion path as the following:

$$W_T = W_C + W_P + W_R \tag{3.1.1}$$

where W_T is the total potential energy, W_C is the Coulombic interaction, W_P is the van der Waals interaction and W_R is the overlap repulsion between closed shell ions.

The total potential energy of a diffusing ion in a crystal is calculated, and it is assumed that ion transport has occurred following the path of minimum total potential energy. According to the shape of the diffusion path (or dimensionality of the passageway of the Li-ion) in the crystal, various structure types can be classified, including 1D unidirectional tunnels ($LiFePO_4$ [104,105]), 2D layered structures ($LiCoO_2$ [105,106]) and 3D arrays of tunnels ($LiMn_2O_4$ [62,107]). The cathode structure type directly influences the Li-ion diffusion values as seen in Tables 11–13 [97,98,100–102,108–130]. $LiCoO_2$, having a 2D layered structure, shows the highest Li-ion diffusivity among the three different cathodes, while $LiFePO_4$ with one-dimensional channels shows the lowest diffusivity.

First-principles calculations [62,104,105,131–133] can be a powerful tool for understanding atomic scale diffusion in cathode particles and providing detailed insight into diffusion mechanisms and structural properties. First-principles calculations of Li_xCoO_2 diffusivity have been conducted at varying intercalation levels of Li ($0 \le x \le 1$), elucidating the reason for the wide variation of diffusivity based upon the activation barrier change and divacancy diffusion mechanisms (also, see Table 7) [131,134]. First-principle calculations were used in [135] to show that (0 1 0) surface termination in $LiFePO_4$ is the most stable orientation and also favors Li-ion diffusion. Theoretical calculations derived from the utilized techniques, however, contain intrinsic inaccuracies [132,136] and originate from the shortcomings of approximation [137] and numerical error [138]. Furthermore, *ab initio* techniques may be problematic or even inapplicable because of impurities, multiple phases [109], and disordered amorphous phases in the host structures [139].

The primary schemes for manipulating the diffusivity in cathode particles include doping, coating the cathode particle surface, scaling down the particle size, and changing the crystallinity (see Tables 11–13). The doping technique is often used by the semiconductor industry in order to precisely alter silicon conductivity by creating charge carriers in the form of excess electrons or holes [140]. Using dopants in cathode materials is based on the same concept. The dopants, in theory, affect the electronic structure of the cathode by changing the crystal parameters [113] with the intent of increasing [114] or decreasing [127] the ease of Li-ion transport. Unfortunately, doping cathodes has not produced any significant improvement in diffusivity; in some cases diffusivity has been increased by an order of magnitude relative to a control sample, although the absolute value still falls within the average measured diffusivity of the material.

While the mechanism is not yet fully understood, coating the surface of the cathode material with a layer of a different substance can increase diffusivity. If a cathode material is coated in a non-conductive material, (e.g., $LiCoO_2$ with $LiFePO_4$ coating) [116], there is no significant change in diffusivity; however, an increase in cycle life is observed as the coating prevents cobalt ion dissolution. If a conductive species (e.g., carbon) is used as the coating material diffusivity is increased, perhaps by enhancing electrical conductivity.

The most straightforward scheme for manipulating diffusivity is to reduce the cathode particle size to the nano-scale to give a reduced diffusion length; this technique has been reviewed in [141]. One drawback to nano-sized cathode particles is that they usually show a higher reactivity than micro-sized particles and therefore more easily form an SEI layer which can act as a diffusion barrier impeding the motion of Li-ions [110,142]. Amorphous phases, like grain boundaries, are known to have larger diffusivity than crystalline phases. Thus, by controlling the ratio between

Please cite this article in press as: M. Park, et al., J. Power Sources (2010), doi:10.1016/j.jpowsour.2010.06.060

Table 14
Electrical conductivity of $LiCoO_2$ under various conditions.

Cathode material	Electrical conductivity ($S\,cm^{-1}$)		Description	Measurement technique	Reference
Li_xCoO_2	• 2.0×10^{-1} (single crystal) • 5.0×10^{2} (single crystal)		• Semiconductive ($x = 1$): conductivity is dependent on T • Metallic conduction ($x = 0.5$): conductivity is independent of T	4 Point Probe DC	[154]
$Li_{1.0}Mg_yCo_{1-y}O_2$	• $10^{-3.75}$: $y = 0$ • $10^{-1.1}$: $y = 0.03$ • $10^{-0.75}$: $y = 0.06$		• Mg doping induces electron holes via $2Co^{2+} \rightarrow Co^{4+} + Mg^{2+}$: NMR study confirms this phenomenon	4 Point Probe DC	[99]
$Li_xNi_{0.30}Co_{0.70}O_2$	• 10^{-3} to 10^{-2}: $0.72 < x < 1$ • $10^{-2.5}$ to $10^{0.2}$: $0.40 < x < 0.72$		• Electrical conductivity: thermally activated process for all x • True metallic behavior not observed: Ni doping hinders electron delocalization	4 Point Probe DC	[155]
$LiGa_yCo_{1-y}O_2$	• 6.76×10^{-4}: undoped sample • 1.30×10^{-3}: doped sample ($y = 0.005$) • 3×10^{-5}: doped sample ($y = 0.1$)		• $y = 0.005$: creates band gap • $y = 0.1$: widening band gap	4 Point Probe DC	[156]
Al_2O_3-coated $LiCoO_2$	• 1.30×10^{-9} (bare) • 6.66×10^{-9} (0.2 wt%) • 1.40×10^{-8} (2.0 wt%) • 1.81×10^{-9} (bare) • 1.11×10^{-8} (0.2 wt%) • 2.00×10^{-8} (2.0 wt%)	Density = $1.8\,g\,cm^{-3}$ Density = $2.0\,g\,cm^{-3}$	• Effect of density and Al_2O_3-coating on electrical conductivity	–	[157]

Please cite this article in press as: M. Park, et al., J. Power Sources (2010), doi:10.1016/j.jpowsour.2010.06.060

Table 15
Electrical properties of $LiMn_2O_4$ under various conditions.

Cathode material	Electrical conductivity (S cm^{-1})		Description	Measurement technique	Reference
$Li_xMn_2O_4$	• $10^{-6.0}$ ($x = 1.00$) • $10^{-5.5}$ ($x = 0.98$) • $10^{-3.6}$ ($x = 0.75$) • $10^{-4.5}$ ($x = 0.40$)		• Effect of deintercalation • Small polaron mechanism is suggested for electrical transport	4 Point Probe AC	[85,86]
$Li_{1+d}Mn_{2-d}O_4$	• 1.6×10^{-2} (at 50 °C): d = 0, bare • 1.4×10^{-2} (at 50 °C): d = 0.005, bare • 5.4×10^{-2} (at 50 °C): heat treated at 580 °C • 1.4×10^{-8} (at 50 °C): heat treated at 800 °C		• Effect of heat treatment and d variation • Valence state varied due to heat treatment temperature • Effect of *d* variation is negligible	EIS	[158]
$Li_xMn_2O_4$	Electrochemical • $10^{-4.8}$ ($x = 0.98$) • $10^{-3.6}$ ($x = 0.75$) • $10^{-4.7}$ ($x = 0.4$)	Chemical • $10^{-4.2}$ ($x = 0.98$) • $10^{-3.7}$ ($x = 0.8$) • $10^{-2.5}$ ($x = 0.4$)	• Different deintercalation processes: electrochemical and chemical • Chemical process induces highly defective structure	4 Point Probe AC	[159]
$LiCo_yMn_{2-y}O_4$	• 2.0×10^{-4} ($y = 0$), 2.0×10^{-2} ($y = 1$): at RT • 2.0×10^{-8} ($y = 0$), 1.0×10^{-4} ($y = 1$): at −107 °C • $10^{-4.2}$ ($y = 0$, to 0.5): at RT • 10^{0} ($y = 0$), 10^{-1} ($y = 0.5$): at 394 °C		• Higher *T*: Mott model (small polaron) • Lower *T*: variable-range-hoping model • Lower *T*: hopping of small polaron • Higher *T*: Co ions lowers activation *E*	2 Point Probe AC 4 Point Probe AC	[160] [161]
$LiNi_yMn_{2-y}O_4$	• 2.0×10^{-4} ($y = 0.1$, crystallite size: 22 nm) • 1.9×10^{-7} ($y = 0.5$, crystallite size: 22 nm)		• Ni^{2+} replaces Mn^{3+}: no electron hopping at higher Ni content (e.g., $y = 0.5$)	2 Point Probe AC	[162]
$LiCu_yMn_{2-y}O_4$	• $2.0 \times 10^{-5.0}$ ($y = 0$ at 17 °C) • $7.0 \times 10^{-4.0}$ ($y = 0.2$ at 17 °C) • $6.0 \times 10^{-3.0}$ ($y = 0.4$ at 17 °C)		• Transport through e_g Mn electron and e_g Cu (t_g Fe) holes	4 Point Probe AC	[163]
C-coated $LiMn_2O_4$	• $10^{-4.0}$ (C: 0.6 wt%, at 30 °C) • $10^{-5.1}$ (C: 2.5 wt%, at 30 °C) • $10^{-6.3}$ (C: 13 wt%, at 30 °C)		• Carbon coating effect on electrical conductivity	4 Point Probe AC	[164]

crystalline and amorphous phases, diffusivity can be tailored [119]. Ultimately, none of these schemes have lead to a breakthrough in ionic conductivity. A critical challenge facing experiments designed to tailor diffusivity is that the measured values vary widely depending on experimental setup, measurement or simulation technique and electrode fabrication method. Thus, in order to evaluate these schemes, it becomes important to know the precise range and cause of diffusivity variation for each host structure.

The maximum charge/discharge rate is one of the important factors for high power applications of Li-ion cells and is directly related to Li-ion conduction properties (diffusivities). Higher diffusivity results in a higher charge/discharge rate. The response of a Li-ion cell to the various charge/discharge rates can be found in CV plots (or diffusivity plots) [118,143–148]; as sweeping voltage increases, current increases or vice versa. From these plots it can be seen that as the rate increases the features observed at

Please cite this article in press as: M. Park, et al., J. Power Sources (2010), doi:10.1016/j.jpowsour.2010.06.060

Table 16
Electrical properties of $LiFePO_4$ under various conditions.

Cathode Material	Electrical Conductivity ($S\,cm^{-1}$)	Description	Measurement Technique	Reference
$Li_{1-x}Cr_xFePO_4$	• 8.0×10^{-10}: $x = 0$, sintered at 700 °C	• Higher conductivity for doped sample; p-type conduction (holes)	2 Point Probe DC	[91,92]
	• 6.0×10^{-9}: $x = 0$, sintered at 850 °C • 1.0×10^{-1}: $x = 0.03$		2 Point Probe AC	
Li_xFePO_4	• 10^{-2}: $x = 0.9$(impurity: $Fe_2P_2O_7$) • 10^{-9}: $x = 1.0$(no secondary phase)	• Effect of synthesis conditions • Impurity increases conductivity	Hall Effect	[165]
	• 10^{-3}: $x = 1.1$ (impurity: Li_3PO_4) • 3.5×10^{-5}: total conductivity, • 3.5×10^{-5}: electrical conductivity	• Single crystal (c-axis, at 146 °C) • Electrical conductivity » ionic conductivity	AC impedance DC polarization	[124]
	• 1.6×10^{-9}: ionic conductivity			
$LiFePO_4$/C composite	• 10^{-7} (size: 20 nm, C content: 16 wt%)	• Effect of nano-sized particle and C coating	–	[166]
	• 10^{-3} (size: 30 nm, C content: 6 wt%)			
$Li_{1-x}M_xFePO_4$ (M = Zr, Nb, Mg)	• 8.0×10^{-9}: undoped samples • $\sim 10^{-2}$: doped samples	• Higher conductivity for doped sample; p-type conduction (holes)	4 or 2 Point Probe DC	[36,167]
C coated-$Li_{0.99}Nb_xFePO_4$	• $\sim 10^{-9}$ • $\sim 10^{-1}$ (4.74 wt% C and $x = 0$) • $\sim 10^{-2}$ (2.50 wt% C and $x = 0$)	• Pure $LiFePO_4$ • Effect of carbon coating; percolation of C coated particles	AC impedance	[168]
	• $\sim 10^{-3}$ (1 wt% C and $x = 0.01$)	• Effect of carbon coating and Nb doping		
C/$LiFePO_4$ composite	• $\sim 10^{-1}$ (30 wt% C), $\sim 10^{-3}$ (17 wt% C) and $\sim 10^{-4}$ (7 wt% C)	• Effect of carbon phase; C added in the beginning of synthesis	2 Point Probe DC	[169]
Fe_2P/Li_xFePO_4 composite	• 1.0×10^{-3} at $x = 0.99$ • 2.0×10^{-4} at $x = 0.97$	• Effect of Fe_2P (metallic inclusion of phosphide) phase	4 Point Probe DC	[170]

lower rates (e.g., distinctive current peaks) disappear and peak current decreases (capacity decreases). This is caused by a limit in ionic conductivity. Another important limiting factor is related to the thermal properties of the cell. Li-ion cells operated at higher charge/discharge rates generate more heat; this can induce structural damage and thus severe capacity loss during cycling. Therefore the maximum charge/discharge rate should be optimized and the operating temperature controlled by an appropriate thermal management scheme.

The difference between charge rate and discharge rate at the same voltage (or driving force) is dependent upon the material system. For example, $LiMn_2O_4$ and $LiFePO_4$ cathodes show smaller differences between charge rates and discharge rates [118,143,145] while $LiCoO_2$ shows quite large differences [146,148]. Common causes of such differences are SEI layer growth rate [118], phase transition [148] and transition in electrical properties (transition between semiconductor to metal) during charge/discharge [146].

Diffusion phenomena with a complex geometries such as dendrite formation, the SEI layer, and electrode deposition are very important in understanding the behavior of Li-ion batteries. To address these problems, the phase field approach is one of the most powerful tools. The key point of the phase field method is treatment of the interface between the phases. The interface is described by a smooth but localized change around the interface. This reduces the mathematical difficulties associated with applying the boundary conditions at the interfaces. The phase field method has been extensively applied to the modeling of microstructure evolution such as grain growth [149], interaction of nanoparticles with lipid layers [150], and control morphology of nanostructures within an electric field [151]. In electrochemistry, the phase field method has been used to explore the equilibrium structure and kinetics of an electric field between two phases consisting of charged components [152,153].

3.2. Electrical conduction in cathode materials

Many studies detailing the electrical conduction of cathode materials have been published. The electrical properties of $LiCoO_2$, $LiMn_2O_4$ and $LiFePO_4$ are summarized in Tables 14–16 [36,85,86,91,92,99,124,154–170]. The ability for the cathode materials reviewed here to intercalate Li-ions is closely related to both their electrical and ionic conduction [38]. Yet compared to the ionic conduction process, electrical conduction is not considered a dominant factor.

Please cite this article in press as: M. Park, et al., J. Power Sources (2010), doi:10.1016/j.jpowsour.2010.06.060

Among many reviews [39,45,171–173] on cathode materials and cell performance limiting factors, attention has been directed to the electrical conductivity of cathode materials for increasing diffusion and ultimately the performance of Li-ion batteries [172]. All cathode materials considered here have semiconductor features. Electrical conduction in a semiconductor is a thermally activated phenomenon and usually follows an Arrhenius type relationship as shown below [174]:

$$\sigma T = \sigma_o \exp\left(-\frac{E_a}{k_B T}\right) \quad (3.2.1)$$

where σ is the electrical conductivity, σ_o is the pre-exponential factor, E_a is the activation energy, k_B is the Boltzmann constant and T is the temperature.

A remarkable jump in electrical conductivity of $LiFePO_4$ using doping methods was reported [36]; later it was questioned whether the enhanced electrical conductivity resulted from the dopants or from carbon residue impurities [175,176]. First-principles calculations [165] show that electronic conductivity of $LiFePO_4$ is not affected by doping (or solid-state reaction conditions). Although the electronic conductivity is found to be between 10^{-3} and 10^{-2} S cm^{-1} for Li_xFePO_4 ($0.7 < x < 0.95$ or $1.05 < x < 1$) when doped, this is attributed to an increase in electronic conductivity (relative to the values found in Table 10) caused by impurities present in the sample. Also, unlike previous reports [36,172], $LiFePO_4$ is actually found to have larger electrical conductivity than ionic conductivity, and thus ionic conductivity dictates electrochemical performance [177]. Unfortunately, in many cases doping decreases electrical conductivity [156,163,178] and does not produce any significant benefit. Thus it remains unclear how the electrical conductivity of $LiFePO_4$ can be increased.

Another dominant factor in changing electrical conduction is phase transition. $LiMn_2O_4$ undergoes a reversible cubic ($Fd3m$) $\Leftrightarrow$ orthorhombic ($Fddd$) phase transformation near room temperature (~280 K) [179,180] inducing a modification of the atomic structure, and thus electrical conductivity. Usually low-temperature orthorhombic phases have lower electrical conductivity [85,180]. $LiCoO_2$ also shows insulator-to-metallic transformation behavior in terms of activation energy [181] when local conducting domains around Co^{3+} become connected via Li-ions in a partially intercalated state. This transition happens when a certain number of Li-ions are deintercalated [7]. The intercalation-induced phase transformations observed in $LiMn_2O_4$ and $LiCoO_2$ exhibit changes in electrical conductivity of about three orders of magnitude [181].

First-principles calculations are advantageous in understanding the electronic structure of cathode particles and the doping effect [82]. The lack of dependable models, however, makes the prediction of electrical conductivity from first-principles calculations much more difficult than comparable diffusivity predictions [131,138]. The reported band gap values of each of the cathode materials considered varies widely; for example the band gap of $LiFePO_4$ has been reported to be between 0.3 and 1 eV [91,92,182] depending on the computational scheme. Also, it is hard to explain why $LiCoO_2$ shows much higher electrical conductivity than $LiFePO_4$ [78,38] by examining the electronic structure (band gap) alone. For spinel (e.g., $LiMn_2O_4$) and olivine (e.g., $LiFePO_4$) cathodes, an often-proposed mechanism is the "hopping of small polarons" common in insulator materials [183–185]. This mechanism is adopted to explain the relatively easier electron charge transfer in these materials, even though the cathode particles have a band gap more properly associated with semiconductors. This example shows the immaturity of theories that have been used so far to understand the electronic conduction and reveals the amount of work left to do.

The only successful scheme to enhance electrical conductivity has been a coating method using nano-sized particles

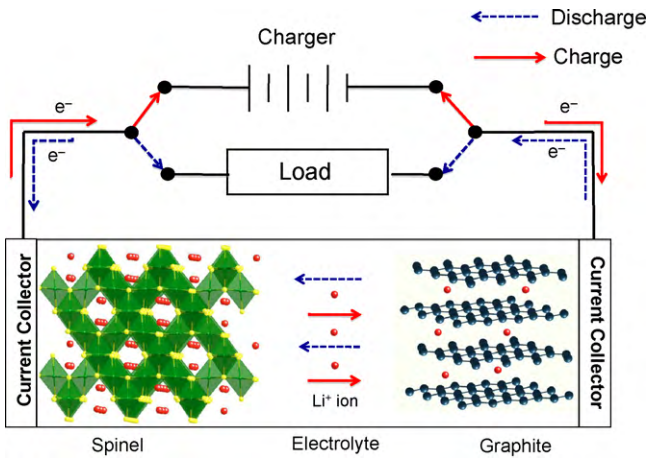

Fig. 4. Operating Li-ion battery.

(Tables 14–16). Considerable research on the effect of coating nano-sized particles on cell performance (capacity or cyclability) has been conducted to date [169,186–189]. However, the underlying mechanisms are controversial and reveal a lack of fundamental understanding. It has been argued that it is not the carbon coating but the smaller size of the particle that brings a significant increase in electrical conduction, due to the larger ionic conductivity of the cathode particles [190]. In some cases [187,191], a combination of surface coating with carbon and transition metal doping has been attempted. Results show better cell performance (e.g., less capacity fading), but the actual mechanism or dominant factor has not been discussed. Overall, understanding the quantitative interaction between ionic and electrical conduction remains incomplete.

4. Survey of conduction studies in anode materials

Although attempts have been made to find suitable replacements, currently only carbonaceous materials are used in commercial anodes [192]. Carbonaceous materials include graphites (natural graphite and HOPG), modified graphites (MCMB, carbon fiber, metal deposited carbon fiber), and non-graphitic carbons [193]. There are a number of reviews on anode materials [193–196] and many of them focus on both carbon and inorganic materials. Conduction properties of carbonaceous materials are primarily reviewed here; other anode materials display conduction mechanisms similar to those described for cathode materials.

Conduction in graphite anodes is complex due to continuous phase transformations and the formation of the SEI layer. Phase transformations are reflected in the open-circuit voltage (OCV) curve as distinct plateaus [197]. Also conduction is strongly dependent upon the degree of crystallinity. As the fraction (f) of amorphous phases (fraction of crystalline phases, $1-f$) increases, electrical conductivity decreases and diffusivity increases. This indicates the possibility of optimizing conduction properties of carbonaceous materials by varying the fraction of each phase [198]. Non-graphitic carbonaceous materials do not undergo phase transformations and therefore do not show distinctive stages in the OCV curve [197]. The SEI layer displays much lower ionic and electronic conductivity than the bulk electrode. To elucidate the mechanisms related to the properties and performance of Li-ion batteries, precise investigation of the electronic state and the diffusion process in the carbon and the SEI layer is still required.

4.1. Ionic conduction in anode materials

Intercalation/deintercalation of Li-ions in graphitized carbon is well established and documented [199–202] (see also Fig. 4). A

Table 17
Diffusivity of Li-ion in graphite under various conditions.

Anode material	Diffusivity ($cm^2\ s^{-1}$)	Description	Measurement technique	Reference
Natural graphite	• 10^{-9} to 10^{-10}: measured at RT • 10^{-11} to 10^{-10}: measured at −35 °C • 10^{-6} to 10^{-5}: dilute stage 1 • 10^{-7} to 10^{-8}: stage 4, 4, and 2L • 10^{-8}: stage 2 and 1 • 10^{-9}: between stage 1 and stage 2 • 10^{-10}: between stage 2 and stage 2L	• Structure of Li-GIC: P_6/mmm •Effect of lower temperature • Diffusivity dependence on stage phenomenon; it keeps changing in discontinuous manner • Features: order and disorder phases, two-phase regions	PSCA AC impedance	[210] [206]
	• 1×10^{-11} (2.5 V) to 4×10^{-10} (0.8 V)	• Novel technique to measure diffusivity: one complementary parameter needed	RPG	[211]
MCMB	• $10^{-11.7}$ to $10^{-9.8}$: new model • $10^{-9.5}$ to $10^{-7.7}$: geometric area	• Surface area calculated by suggested model • Diffusivity trend is different even in the same method when geometric surface area used	GITT	[212]
Graphitized MCMB	• $10^{-9.1}$ to 10^{-11}: geometric area • 10^{-10} to 10^{-9} ($0.15 < x < 0.8$): insertion • 10^{-10} to 10^{-8} ($0.15 < x < 0.8$): extraction	• 0.025 V < E/V vs. Li/Li^+ < 0.25 V • Novel technique to measure diffusivity: no complementary parameter needed	Potential relaxation	[213]
Graphite	• 1×10^{-11} to 1×10^{-7}: (0.025 V < E/V vs. Li/Li^+ < 0.25 V)	• Discussion on PITT method for the diffusivity of two-phase regions	PITT	[214]
HOPG	• 1.14×10^{-12}, 3.84×10^{-11}: bulk • 1.42×10^{-12}, 1.82×10^{-11}: powder • 5.36×10^{-12}, 5.89×10^{-11}: bulk • 0.70×10^{-12}, 0.30×10^{-11}: powder	• Diffusivities measured at 0.05 V and 0.2 V vs. Li/Li^+ respectively	EIS PSCA	[207]

prominent feature of graphite anodes is the staging phenomenon related to the intercalation process [203,204]. The domain model has been suggested [199], and the phase diagram for a staged intercalation compound using mean field theory has been calculated [205]. It has also been shown how repulsive forces in a mixed stage can result in a pure stage during intercalation [200]. The diffusivity of Li-ions in graphite is complicated by the constant phase change in the Li-graphite intercalation compound (Li-GIC), which can introduce disorder into the originally ordered structure [206]. As the degree of intercalation increases, diffusivity becomes smaller [207]. For this reason, diffusivity is reported as a function of intercalation or electrode voltage [206]. Note that low quality carbon, which has low crystallinity, does not exhibit the staging phenomenon.

Carbonaceous materials' properties largely depend on the starting materials (carbon precursor), heat treatment, the final mixture ratio between turbostratic and graphitized phases, and/or the straining of fibers during heat treatment [208]. Amorphous carbon is known to be composed of small carbon sheets [209], and is of interest due to a much higher capacity than graphitized carbon. Li-ion diffusivity in amorphous carbon has been calculated to be $5.40 \times 10^{-6}\ cm^2\ s^{-1}$ at 300 K; Li-ion diffusivities in graphite and modified graphite materials are summarized in Tables 17 and 18 [206–208,210–219]. Note that Li-ion diffusivity in amorphous carbon is generally much greater than that in graphitized carbon.

The diffusion process can vary widely from one type of carbon to another [220–222]. Surface modification of carbon by mild oxidation, deposition of metals, and coating with polymers or other kinds of carbons has been shown to increase cell performance (e.g., reversible capacity) [195,223]. Boron doped graphite has also been researched as an option to enhance electrochemi-

Table 18
Diffusivity of Li-ion in modified graphite under various conditions.

Anode material	Diffusivity ($cm^2\ s^{-1}$)	Description	Measurement technique	Reference
Mesophase-carbon fiber	• 2.0×10^{-8}, 1.0×10^{-8} (ordered, disordered phase): pristine fiber	• High Li ion loading capacity	PSCA	[215]
	• 3.5×10^{-8}, 2.0×10^{-8} (ordered, disordered phase): HTT = 250 °C	• Effect of heat treatment		
	• 8×10^{-8}, 5×10^{-8} (ordered, disordered phase): Ag film coating and HTT = 350 °C	• Effect of Ag deposition and/or heat treatment		
	• 1×10^{-10} to 9×10^{-7} (Ag film coating) 0.025 V < E/V vs. Li/Li^+ < 0.6 V		Potential Step	[216]
PAN-based carbon fiber	• 10^{-14} to 10^{-11} (Li_xC_6: $0.1 < x < 0.8$)	• Heat treatment and tension realigns molecular chain	CPR	[208]
Coal pitch-based carbon fiber	• 10^{-12} to 10^{-10} (Li_xC_6: $0 < x < 0.6$)	• CPR: evaluate diffusivity near surface	CPR	[217]
	• 10^{-13} to 10^{-10} (Li_xC_6: $0 < x < 0.6$)	• PSCA: evaluate whole diffusion process	PSCA	
Mesophase pitch-based carbon fiber	• 10^{-9} to 10^{-8} (Li_xC_6: $0.1 < x < 0.5$, HTT = 2000 °C)	• Effect of texture and degree of graphitization	EIS	[218]
	• 10^{-8} to 10^{-7} (Li_xC_6: $0.1 < x < 0.5$, HTT = 3000 °C)			
Disordered Structure-MCMB	• 10^{-8} to 10^{-9} ($0.1 < x < 1$)	Dependence of D_{Li} on intercalation	PSCA	[219]

Table 19
Electrical conductivity of graphite, Li-GIC and a-carbon under various conditions.

Anode material	Electrical conductivity ($S\ cm^{-1}$)	Description	Measurement technique	Reference
Graphite	• 1.89×10^4 (predicted value)	• Parallel direction with respect to graphene layer	–	[75,93,246,247]
	• 1.0×10^4 (single crystal)	• Perpendicular direction with respect to graphene layer		
	• 2.1×10^2 (predicted value)	• Crystallite boundaries limit electrical conduction		
	• 1.0×10^0 (single crystal)			
	• 1×10^3 (polycrystalline graphite)			
Li-GIC	• 2.45×10^5	• Stage 1	–	[245]
Graphite thin film	• 2.5×10^2: bulk graphite	• GB interconnection resistance	4 Point Probe	[80]
	• 3.0×10^1: ten-layers of thin film			
a-Carbon thin film	• 10^2: as-fabricated sample	• Effect of pressure on ionic conductivity of thin film deposited by plasma assisted CVD	4 Point Probe	[248]
	• 10^4: pressurized sample (under 3 GPa)			
PAN-based carbon fiber	• 2.2×10^1 to 2.6×10^1 (tension, 0 MPa)	• Tension under heat treatment induces alignment of molecules and varying electrical conductivity	Linear sweep voltammetry	[208]
	• 4.1×10^1 to 4.6×10^1 (tension, 4.87 MPa)	• HTT = 1100 °C		
	• 4.3×10^1 to 4.8×10^1 (tension, 10.97 MPa)			
	• 4.4×10^1 to 4.7×10^1 (tension, 15.03 MPa)			

Please cite this article in press as: M. Park, et al., J. Power Sources (2010), doi:10.1016/j.jpowsour.2010.06.060

Table 20
Generic thermal models.

No.	Model	Governing equation	Comments	Reference
1	Electrical-electrochemical-thermal coupled model	$\nabla \cdot (k_a \nabla T) + \frac{\Lambda^2}{f_a^2 h R_s} H(x,y) = \rho \hat{C}_{pa} \frac{\partial T}{\partial t}$	• Single Cell, 2D • Perturbation approach • Analytical solution	[257]
2	Electrical-electrochemical-thermal coupled model	$\rho \hat{C}_p \frac{\partial T}{\partial t} = k_{heat,x} \frac{\partial^2 T}{\partial x^2} + k_{heat,y} \frac{\partial^2 T}{\partial y^2} + q_{heat} - q_{conv}$	• Single Cell, 2D • Position, DOD considered • Numerical solution	[255]
3	Electrical-electrochemical-thermal coupled model	$q_{heat} = \sum_j k_{heat}(T_i - T_j) + M_i \frac{dT_i}{dt}$	• Single Cell, 1D • Lumped node model • Numerical solution	[256]
4	Thermal model	$\rho \hat{C}_p \frac{\partial T}{\partial t} = k_{heat,x} \frac{\partial^2 T}{\partial x^2} + k_{heat,y} \frac{\partial^2 T}{\partial y^2} + k_{heat,z} \frac{\partial^2 T}{\partial z^2} + q_{heat}$	• Cell Stack, 3D • q assumed to be constant • Numerical solution	[30]
5	Energy balance-electrochemical-thermal coupled model	$\frac{\partial(\hat{C}_p T)}{\partial t} = \nabla \cdot (k_{heat} \nabla T) + q_{heat}$	• Single Cell, 1D • Numerical solution	[258]
6	Energy balance model	$\Delta H = \frac{1}{2 c_{B,\infty} \bar{V}_{B,\infty}} \frac{\partial \bar{H}_A}{\partial c_A}\Big\|_{\infty} \int (c_A - c_{A,\infty})^2 d\nu + C_{p\infty} \Delta T$	• Single Cell, 1D • heat of mixing • Numerical solution	[259]
7	Energy balance model	$q - IV = \sum_1 \left[I_1 T^2 \frac{d(U_{1.avg}/T)}{dt} \right] - \sum_j \frac{d}{dt} \left[\int_{Vj} \sum_i c_{i,j} R_g T^2 \frac{\partial}{\partial T} \ln \left(\frac{\gamma_{i,j}}{\gamma_{i,j}^{avg}} \right) d\nu_j \right] - \sum_{j,j \neq m} \sum_i \left[\left(\Delta H^o_{ij \to m} - R_g T^2 \frac{d}{dT} \ln \frac{\gamma_{i,m}^{avg}}{\gamma_{i,j}^{avg}} \right) \frac{dn_{i,j}}{dt} \right] + \frac{dT}{dt} \left[\sum_j \sum_i n^o_{i,j} \bar{C}^{avg}_{Pi,j} + \sum_1 \frac{\int_0^t I_1 dt}{n_1 F} \Delta C_{P1} + \sum_{j,j \neq m} \sum_i (\bar{C}^{avg}_{Pi,j} - \bar{C}^{avg}_{Pi,m})(n_{i,j} - n^o_{i,j}) \right]$	• Single Cell, 1D • Numerical solution	[269]

Please cite this article in press as: M. Park, et al., J. Power Sources (2010), doi:10.1016/j.jpowsour.2010.06.060

Table 21
Physical properties of organic carbonate solvent [269–271].

Physical property	Carbonate solvent			
	EC	PC	DEC	DMC
Viscosity (cP)	1.85 (40 °C)	2.53 (30 °C)	0.585 (25 °C)	0.748 (25 °C)
Relative dielectric constant	89.6 (40 °C)	64.4 (30 °C)	3.12 (25 °C)	2.82 (25 °C)
Donor number	16.4	15.1	–	15.1
Molecular structure	Cyclic	Cyclic	Linear	Linear

cal performance [224,225]. Scaling down the particle size, while effective for improving diffusivity in cathode materials, may not be an option in carbonaceous anode materials, as the increased surface area leads to higher lithium consumption during SEI formation. As an example, in spite of their nano-size diameter dimension and other superior material properties, carbon nanotubes (CNTs) are not successful as anode materials [196,226], due to the ease with which the SEI film forms on their surface. Reports on these various modification schemes for carbon materials usually lack a good understanding of the diffusion process. Diffusivity is relatively infrequently reported and when it is, values vary widely (Table 18). Most frequently, reports on Li-ion diffusivity address improving measurement techniques and not the diffusion mechanism itself. This may derive from the complexity caused by the SEI film [227], the staging phenomenon of graphite, and the various phase mixtures mentioned previously.

Due to the ease with which the SEI film forms on anodes, it is important to understand ionic conduction at this interface, since it is closely related to power performance (fast charge/discharge), degradation and safety. To explain the SEI film, most studies use an analogy to passivation films that appear in corrosion [228–230]. Although passivation films are good ionic conductors [229], films as thin as 30 Å can greatly reduce the rate of corrosion by hampering electron-transfer [230]. Similarly, the SEI film is ionically conductive but electronically insulating; it is known that Li-ions can pass through this film [238] and the diffusion mechanism of Li-ions is thought to be defect-mediated (Shottky and Frenkel). The structure and chemical composition of the SEI on Li metal is reported to be similar to the passivation film formed on the same substrate [236]; however, the structure of the SEI film on carbon varies more widely due to the various morphologies of the carbon surface (e.g., basal and cross-section) [231]).

The main components of the SEI are the reduced components of the electrolyte solvents and salts, including Li_2CO_3, lithium alkyl carbonate, lithium alkyloxide, and other salt moieties such as LiF [232]. The structure of the SEI film is affected by current density, various additives in the electrolyte [232,233], temperature, solvents and the Li salt used [232,234,235]. The average resistance of SEI films is reported to be in the range of 10–1000 $\Omega\,cm^2$ and the resistance of grain boundaries are in the range of 10–100 $\Omega\,cm^2$ for a thickness of 10 nm [236]. Thus, grain boundary effects should not be neglected (see Fig. 2). The resistivity of a 30–50 Å SEI film is

Table 22
Ionic conductivity and features of Li salt solutions [41,274–277].

Salt	Solvent	Ionic conductivity[a] ($S\,cm^{-1}$)	Description
$LiClO_4$	PC	5.6	• Lithium perchlorate • Satisfactory solubility and high conductivity • High anodic stability and generates a lower impedance SEI • Less hygroscopic and stable to ambient moisture • Strong oxidant: readily reacts with most organic species at high temperature and high current
	EC/DMC	8.4	
$LiAsF_6$	PC	5.7	• Lithium hexafluoroarsenate •The SEI formed on anode is very stable during cell operation • Excellent anodic and cathodic stability • Toxic
	EC/DMC	11.1	
$LiBF_4$	PC	3.4	• Lithium tetrafluoroborate • Less toxic than $LiAsF_6$ and safer than $LiClO_4$ • Good stability at low and high temperature • Moderate ionic conductivity
	EC/DMC	4.9	
LiTf	PC	1.7	• Lithium trifluoromethanesulfonate • Highly resistant to oxidation • Thermally stable, nontoxic, and stable to ambient • Outperforms $LiPF_6$ when used with carbon fiber (anode) • Poor ionic conductivity and generates a thick and resistive SEI film • Causes severe Al corrosion
LiIm	PC	5.1	• Lithium bis(trifluoromethanesulfonyl)imide • Safe, thermally stable and highly conducting • Causes severe Al corrosion
	EC/DMC	9.0	
$LiPF_6$	PC	5.8	• Lithium hexafluorophosphate • Combination of well-balanced properties: only successfully commercialized salt • Sensitive to ambient moisture and solvents • Thermally unstable at high temperature • Causes tremendous difficulty in preparation and purification
	EC/DMC	10.7	

[a] All samples referenced are 1 mol dm^{-3} solutions of their respective salts

Please cite this article in press as: M. Park, et al., J. Power Sources (2010), doi:10.1016/j.jpowsour.2010.06.060

Table 23
Ionic conductivity of various solid-state electrolytes: I. Polymeric.

Type	Ionic conductivity ($S\,cm^{-1}$)	Description	Measurement technique	Reference
Wet polymer	• 8.46×10^{-8} ($LiPF_6$ 5 wt% in PVdF) • 2.34×10^{-6} ($LiPF_6$ 10 wt% in PVdF) • 2.10×10^{-5} ($LiPF_6$ 15 wt% in PVdF) • 2.70×10^{-4} ($LiPF_6$ 20 wt% in PVdF)	• Complex film (PVdF + $LiPF_6$) impregnated with EC:PC (1:1)	EIS	[287]
Gel-polymer	• 7.9×10^{-3} (at 30 °C) • 9.4×10^{-8} (at 30 °C) • 1.2×10^{-5} (at 30 °C) • 8.0×10^{-6} (at 30 °C)	• EC:DEC (1:2) and $LiPF_6$ (1 M) • ST-BD (60:40) swollen by electrolyte • 2EHA-AN (85:15) swollen by electrolyte • 2EHA-AN (75:25) swollen by electrolyte	EIS	[288]
Gel-polymer	• ~ 10^{-4}: EMITFSI (at 30 °C) • ~ 10^{-2}: EMITFSI + LiTFSI (at 30 °C) • ~ 10^{-4}: HTMATFSI (at 30 °C) • ~ 10^{-3}: HTMATFSI + LiTf (at 30 °C)	• PEO–PMA (7:3) swollen by ionic liquid or ionic liquid based electrolyte	EIS	[289]
Li-ion conducting polymer	• 8.0×10^{-8} • 1.0×10^{-8}	• PEO (polymer): host material • SiO_2 (inorganic filler; plasticizer) and $LiBF_4$ (Li salt) are added to PEO	EIS	[290]
Plastic crystal	• 1×10^{-4} (4%), 5×10^{-5} (15%): $LiBF_4$ • 6×10^{-4} (4%), 1×10^{-3} (15%): LiIm	•Succinoitrile doped by Li salts	EIS	[291]

PEO: poly(ethylene oxide); ST–BD: styrene-butadiene; PEO–PMA: poly(ethylene oxide)–poly(methyl methacrylate); 2EHA-AN: 2-ethylhexyl-acrylate-acrylonitrile; EMITFSI: 1-ethyl 3-methyl imidazoliumbis(trifluoromethanesulfone)imide; HTMATFSI: hexyltrimethylammoniumbis(trifluoromethanesulfone)imide.

reported to be 3 to $4 \times 10^8\ \Omega\,cm^2$ [237]. Although the resistance is assumed to be ionic resistance, there remains insufficient knowledge about the diffusion mechanism and diffusivity of Li-ions in the SEI. The conduction mechanism of interfacial film on cathode materials ($LiMn_2O_4$ [238], $LiCoO_2$ [239], and $LiFePO_4$ [240,241]) and surface coatings [242–244] (metallic, non-oxide, oxide and carbon) has not been as thoroughly investigated as the SEI layer on carbon anodes. In some cases it has been reported that Li-ions go through the coating layer [243] but the detailed mechanism of the Li-ion conduction is not clear and still under investigation.

Table 24
Ionic conductivity of various solid state electrolytes: II. Crystalline.

Type	Ionic conductivity ($S\,cm^{-1}$)	Description	Measurement technique	Reference
Crystalline (perovskite)	• 1.0×10^{-3} ($x = 0, 0.1$) • 1.0×10^{-8} ($x = 0.3$) • 1.0×10^{-11} ($x = 0.4$)	• Solid solution, $xLaAlO_3$–$(1-x)La_{0.5}Li_{0.5}TiO_3$: amount of $LaAlO_3$ (x) is varied	EIS	[292]
Crystalline (NASICON)	• 6.7×10^{-7} (at 250 °C)	• Phosphate compound ($Li_2AlZr[PO_4]_3$): effect of substitution of Al and Zr for Ti in $Li_2Ti_2[PO_4]_3$	EIS	[293]
Crystalline (thio-LISICON)	• 4×10^{-6} ($x = 0$) • 5×10^{-6} ($x = 0.05$) • 4×10^{-7} ($x = 0.1$) • 2×10^{-9} ($x = 1$)	• $Li_{4-2}xZn_xGeS_4$ • Composition dependent ionic conductivity	EIS	[294]
Crystalline	• 5×10^{-4} ($x = 0$) • 5×10^{-5} ($x = 2.0$) • 4×10^{-4} ($x = 3.0$) • 5×10^{-7} ($x = 4.0$)	• Chlorine compound ($Li_3InBr_{6-x}Cl_x$): effect of substituting Br with Cl	EIS	[295]
Crystalline (Garnet)	• 5×10^{-5} • 5×10^{-4} • 5×10^{-4} • 5×10^{-3}	• Pristine sample: $Li_5La_3Ta_2O_{12}$ • Substituting La with Ca: $Li_6CaLa_2Ta_2O_{12}$ • Substituting La with Sr: $Li_6SrLa_2Ta_2O_{12}$ • Substituting La with Ba: $Li_6BaLa_2Ta_2O_{12}$	EIS	[296]

Please cite this article in press as: M. Park, et al., J. Power Sources (2010), doi:10.1016/j.jpowsour.2010.06.060

Table 25
Ionic conductivity of various solid state electrolytes: III. Glassy.

Type	Ionic conductivity ($S\,cm^{-1}$)	Description	Measurement technique	Reference
Glass (LiPON)	• 1.8×10^{-6} to 8.0×10^{-7}	• Effect of RF power on ionic conductivity (2.2–5.7 $W\,cm^{-2}$)	AC impedance	[297]
	• 8.0×10^{-7} to 1.8×10^{-6}	• Effect of N_2 gas pressure (0.5–2 Pa)		
	• 9.0×10^{-7} to 5.0×10^{-7}	• Effect of target–substrate distance (7–11.5 cm)		
	• 2.5×10^{-7} to 8.0×10^{-7}	• Effect of target density (1.48–2.22 $g\,cm^{-3}$)		
Glass	• 1.2×10^{-4} (25 kpsi)	• Sulfide-based Li glass: $0.375SiS_2–0.375Li_2S–0.25LiCl$	AC impedance	[298]
	• 2.0×10^{-4} (50 kpsi)	• Effect of isostatic pressure on ionic conductivity		
	• 3.0×10^{-4} (125 kpsi)			
Composite (glass + polymer)	• 5×10^{-3}	• Sulfide-based Li glass: $0.36SiS_2–0.63Li_2S–0.01Li_3PO_4$	AC impedance	[299]
	• 1×10^{-3} (dry process)	• Sulfide-based Li glass particles + SBR (8 vol%)		
	• 1×10^{-4} (wet process)	• Sulfide-based Li glass particles + SBR (4 vol%)		
Glass-ceramics	• 1.12×10^{-8}	• Glass; $Li_2O–Al_2O_3–TiO_2–P_2O_5$	AC impedance	[300]
	• 6.53×10^{-4}	• Glass–crystalline mixed phase; $Li_{1+x}Al_xTi_{2-x}(PO_4)_3$, $x = 0.3$		
	• 5.98×10^{-9}	• Glass; $Li_2O–Al_2O_3–GeO_2–P_2O_5$		
	• 3.99×10^{-4}	• Glass–crystalline mixed phase; $Li_{1+x}Al_xGe_{2-x}(PO_4)_3$, $x = 0.3$		
	• 1.00×10^{-3}	• Glass–crystalline mixed phased by heat treating ($30P_2S_5–70Li_2S$) glass	AC impedance	[301]

4.2. Electrical conduction in anode materials

The electronic structure of graphite has been researched for more than 60 years since a paper dealing with the band structure and the anisotropic electrical conductivity of graphite was published [93]. Graphite is known as a zero band gap semi-metal due to its unique conduction behavior under the influence of electrical fields [78,79]. Interlayer forces are small (van der Waals force), and the distance between graphene layers is large (3.35 Å) [61] allowing Li-ions to easily diffuse between graphene sheets. The intercalation affects both the crystal and electronic structures. Electrical conductivity of the Li-GIC increases with increasing intercalation levels, due to the electron donor nature of the Li. This is the opposite of ionic conduction in which diffusivity decreases due to the insertion of Li-ions. The electrical properties of various Li-GICs and carbonaceous materials [245] are summarized in Table 19 [75,80,93,208,245–248]. In the case of amorphous carbon, as the disorder increases, electrical conductivity significantly decreases. While first-principles calculations are not applicable for analyzing the electronic structure of amorphous carbon, various models considering hybridization of sp^3 and sp^2 molecular orbitals have been developed to predict electrical conductivities in this material [249,250].

A short circuit might be construed to be an unintentional case of very high conduction for a Li-ion battery. Classically, a short circuit is defined as a circuit element across which the voltage is zero, regardless of the current flowing through it (electrical resistance approaches zero; the opposite of short circuit is open-circuit) [251]. Consequences include excessive electric current flow, causing circuit damage, overheating, fire or explosion. From a safety point of view, internal or external short circuits of Li-ion batteries [252] are very important because these can cause a sudden increase in heat generation called thermal runaway [253]. Depending on cell design, up to 70% of the entire energy of the cell can be released in less than 60 s causing significant self-heating of the cell [254]. Although the short circuit phenomenon itself is not the main subject of modeling, many thermal models have been made to predict temperature increase due to various factors including short circuit. These models address a single cell [254,255] and/or cell stacks [30,256] coupling with an electrochemical model or experimental data. Various mathematical models have been summarized as a table (see Table 20) and included here [30,255–260].

5. Survey of conduction studies in electrolytes

The ideal electrolyte for Li-ion batteries has not yet been developed; although organic electrolytes are widely used due to their higher ionic conductivities and practical operating temperature range, there are many reasons to develop alternatives. While various material systems have been explored and tested as replacements, most do not display a sufficient ionic conductivity to be utilized in Li-ion batteries; a room temperature conductivity of at least $10^{-3}\,S\,cm^{-1}$ is needed for an electrolyte to function well in consumer battery systems [261]. Research in this area reveals the complex nature of the problem and the difficulty of understanding the ionic transport mechanisms due to the many parameters involved (e.g., viscosity, salt concentration, solvation, ion association and ion–solvent interaction). There are currently no reliable theories for developing new electrolytes; theories developed in previous research suggest results that cannot be reproduced experimentally [262].

5.1. Organic electrolytes

The role of the electrolyte is to provide an ionic conduction path between the anode and the cathode. Thus, the prime concern in electrolyte research is to enhance ionic conductivity [263,264]. When Li salts (e.g., $LiPF_6$) are dissolved in a solvent, cations (Li^+) and anions (PF_6^-) are produced. Dissociation of the salt is closely related to the dielectric constant of the solvent, with a high dielectric con-

stant indicative of strong solvating power [265]. Solvation occurs because the Li-ion is entirely surrounded by solvent molecules reducing the influence of the anion. Salts with large anions are advantageous for conductivity and solubility because they better distribute their negative charge, preventing ionic pairing [262]. The viscosity determines the motion of ions; low viscosity facilitates ionic movement [266]. Cationic (Li^+) transport in electrolytes, as dictated by the viscosity and solvating power of the solvents, is expressed as the transport (t^+) and transference (T^+) numbers. The transport number, as expressed by Eq. (5.1.1) [267] is defined as the net charge carried by the cations out of the total charge carried by both the cations and anions passing across a reference plane:

$$t^+ = \frac{i_+}{i_+ + i_-} = \frac{i_+}{i_t} = \frac{u_+}{u_+ + u_-} = \frac{D_+}{D_+ + D_-} \quad (5.1.1)$$

where i_+ and i_- are the currents carried by the cations and the anions, respectively, i_t is the total current, and $u_\pm$ and $D_\pm$ are the mobility and the diffusion coefficients of the cations and the anions, respectively.

In reality, one measures not only cations and anions but also the associated solvent molecules, which induce drag (i.e. resistance). Thus, instead of transport number, transference number is used. The transference number of a Li-ion is measured experimentally [268] using the following equation [306]:

$$T^+_{Li^+} = \frac{R_b}{\Delta V/I(\infty) - R_{ct}} \quad (5.1.2)$$

where ΔV is the polarization voltage, $I(\infty)$ is the steady state current after polarization, R_b and R_{ct} are the bulk resistance and charge transfer resistance, respectively, in the complex impedance spectra before polarization.

It is difficult for a single solvent system to display both a high dielectric constant and a low viscosity (Table 21 [269–271]); therefore, many researchers have explored mixtures of solvents [263,264,266,272] to develop an advanced liquid electrolyte for Li-ion batteries. The following equation represents a binary solvent system [264]:

$$m(\text{Li salt; e.g. } LiPF_6) + (1-w)(\text{solvent A; e.g. PC}) + w(\text{solvent B; e.g. DEC}) \quad (5.1.3)$$

where m is the amount of Li salt in molality (mol kg^{-1}) and w is the weight fraction.

When predicting conductivity and viscosity of a single solvent it is difficult to find a reliable theory; only empirical relations for a solvent system have been proposed. The Jones–Dole (JD) (Eq. (5.1.4)) and Debye–Hückel–Onsager (DHO) equations (Eq. (5.1.5)) for viscosity and conductivity for a single solvent system [262] are shown as follows:

$$\mu_r = \frac{\mu}{\mu_o} = 1 + AC^{1/2} + BC + DC^2 \quad (5.1.4)$$

where μ_r is the relative viscosity, μ is the viscosity of solution, μ_o is the viscosity of pure solvent, C is the concentration of salt and A, B, D are coefficients:

$$\Lambda = \Lambda_o - SC^{1/2} \quad (5.1.5)$$

where Λ is the molar conductivity, Λ_o is the molar conductivity at infinite dilution, S is the parameter depending on both the physical properties of the solvent and the nature of the electrolyte and C is the solute concentration.

If the identity of the salts or solvents is changed, these empirical equations are no longer directly applicable and should be modified. The equations become more complicated for a mixed solvent system. Therefore, when developing a new multi-solvent system, the properties of electrolytes are determined experimentally. The temperature dependence of conductivity is fitted using a Vogel–Tamman–Fulcher (VTF) type equation (Eq. (5.1.6)) [272]. The VTF type equation is a deviation from an ideal Arrhenius type equation, and the plot usually shows a convex shape [273]:

$$\kappa = \frac{A}{\sqrt{T}} \exp\left(-\frac{E_a}{R}\frac{1}{T - T_o}\right) \quad (5.1.6)$$

where A is the constant, E_a (kJ mol^{-1}) is the activation energy and T_o (K) is the theoretical glass transition temperature. Here A, E_a and T_o are the fitting parameters.

The ionic conductivity of various Li salts in PC and EC/DMC solvents at RT, and the important features of each electrolyte formulation, are summarized in Table 22 [41,274–277]. Note that estimating the diffusivity of Li-ions using the Nernst–Planck equation (see Eq. 5–7 in Table 8) can produce an overestimate because ionic conductivity arises from both cations and anions [278]. The precise value of diffusivity of Li-ions should be selectively measured by experimental methods, for example NMR [266]. Although the conductivity of the electrolyte is the most crucial and fundamental factor, other aspects such as formation and properties of the SEI layer [269,279], stability on the cathode and anode surfaces [263], stability at high temperatures [280,281], stability at high current rates [282], and toxicity [283] should also be considered. Depending upon application these factors may be more decisive than conductivity on electrolyte suitability.

5.2. Solid-state electrolytes

Solid-state electrolytes have many advantages over liquid electrolytes, including: a simple design, a natural seal, resistance to shock and vibration, resistance to pressure and temperature variations, a wider electrochemical stability and better safety [284–286]. These materials, however, still suffer from relatively lower ionic conductivity [261]. Broadly speaking, solid electrolytes are classified as gelled (or wet) polymers, solvent free polymers, inorganic crystalline compounds, and inorganic glasses [54]. Ionic conductivities of some of the representative solid-state electrolytes are summarized in Tables 23–25 [287–301]. Ionic conduction in inorganic crystalline compounds is due to the mobile ions hopping among energetically favorable sites in the surrounding potential, as previously discussed. The motion of the surrounding ions simply provides the activation energy for mobile ions to move through channels in the crystalline framework.

The conduction mechanism of polymeric electrolytes (gelled polymers and solvent free polymers) is substantially different from that of inorganic crystalline materials [302] and liquid type electrolytes. In the case of solvent free polymer electrolytes, the motions of the polymer host are responsible for the ionic mobility; ions move only if polymer segments undergo fairly large-amplitude motions [285,302,303] related to the glass transition temperature (T_g). Polymer electrolytes show fast ionic conduction above their T_g where they are largely comprised of amorphous phases. Thus, a low T_g polymer like PEO (polyethylene oxide; T_g, −50 to −57 °C [304]) has become an important polymer host for solvent free electrolytes, and amorphization of this polymer is being researched [285,305,306] as a way to increase its ionic conductivity. Gelled polymers show faster ionic conduction than solvent free electrolytes, due to the diffusion of low molecular weight solvents in polymers [307,308] as well as the motion of polymer segments, as mentioned above.

Solid electrolytes based upon thin film technology developed in the semiconductor industry have been studied intensively as a key component of solid-state microbatteries. The cost of most crystalline and glass electrolytes developed for microbatteries is too high due to long synthesis times and the high temperatures required during fabrication [309]. In addition to these disadvantages, inorganic materials used for solid-state electrolytes often

Please cite this article in press as: M. Park, et al., J. Power Sources (2010), doi:10.1016/j.jpowsour.2010.06.060

contain expensive metals such as Ge, Ti, Sc, In, Lu, La and Y [309]. Due to the difficulties mentioned for scale-up and application of most solid-state electrolytes, only gelled polymer electrolytes have seen commercial success, albeit limited [261,310].

5.3. Ionic liquid electrolytes

Another category of materials considered as electrolytes is ionic liquids – salts with a below-room temperature melting point [311] – because they possess unique properties [311–314] including non-flammability, low vapor pressure, high thermal stability, good electrochemical stability, low toxicity, and high ion content. Physiochemical properties of various ionic liquids can be found in the literature [312–315]. Overall, the viscosities of ionic liquids are one to two orders of magnitude higher, and thus the ionic conductivities are three to four orders of magnitude lower, than those of liquid electrolytes [313,316]. The Walden rule [317] is often used for the relationship between conductivity and viscosity of ionic liquids and is expressed as the following:

$$\Lambda\mu = \text{constant}, \quad \text{where } \Lambda = \Sigma\lambda_i \tag{5.3.1}$$

where λ_i is the ionic conductivity of ion species i and η_v is the viscosity.

Although the Walden rule is similar to the Einstein–Stokes relation (Eq. 3 in Table 7) in its interpretation, the Einstein–Stokes relation is appropriate for non-viscous liquids (e.g., dilute liquid electrolyte) while the Walden rule applies to viscous liquids (e.g., pure ionic liquid [317] or high concentration liquid electrolyte [262]). Much effort has been focused on understanding interactions among ionic species in ionic liquids because viscosity is largely dependent upon these interactions as dictated by various parameters [317] – van der Waals interactions, conformational degrees of freedoms [318], Coulombic forces and the shape of ions. In addition to low ionic conductivities, a low tendency to form an SEI layer on carbonaceous anodes [313,314,319] leads to continuous Li-ion depletion on cycling; in many cases, ionic liquids need additives to be useful as electrolytes [320,321].

6. Concluding remarks and future perspectives

Conduction has been one of the main barriers to further improvements in Li-ion batteries and is expected to remain so for the foreseeable future. In the current review, various aspects of this problem have been discussed for each of the major components of a Li-ion battery (cathode, anode and electrolyte). Efforts to optimize the electrical and ionic conductivity in the cathode have focused largely on doping methods to improve the electrical conductivity and by extension the ionic conductivity. Surface coating cathode particles with a conductive material and/or using scaled down particles have proven to be viable methods to enhance electrical conductivity. Both mathematical treatments [18,19] and recent demonstrations [322–328] suggest that fibrous architectures may be preferred.

Major features of conduction in the anode are closely related to phase transformations as a function of Li-ion intercalation and SEI layer formation. Optimization between crystalline and amorphous phases is an important strategy for tailoring conductivity in carbonaceous electrodes. Efforts to replace conventional organic electrolytes will and must continue, spanning liquid, gel and solid systems.

Modeling is an important and critical element of Li-ion battery research. It is critical to use multi-scale simulations to design superior materials and battery cells, with the understanding that careful and considered reduction of order in modeling is necessary for efficiency, as these models are implemented to control devices. Future efforts to optimize conduction in the various cell components will require coupled models and experiments. Though the review provided here provides some necessary parameters for modeling given the present state of the art, it also highlights gaps in the scientific literature in reported values that must be addressed with new and improved experiments. Diffusivity in particular has been measured via multiple experimental schema, each with its own advantages and disadvantages, but perhaps even more importantly, with intrinsic uncertainties and errors specific to the technique. Continuing to aggressively pursue multi-scale experimental validation of key materials parameters is thus necessary, so that parameters used are thoroughly vetted at these scales, and can be used with confidence in optimizing materials and battery cells.

Perhaps the most important concept that we wish to convey with this review is that theoretical/simulation approaches considering both ionic and electronic conduction are critically needed to properly predict battery performance including, for example, capacity fading and the variation of maximum charge/discharge rate. This review has attempted to address the coupling of ionic and electronic conduction. Entirely unified theories for the relationships of these parameters are not presently available, though development of these are on-going and significant topics and we believe that theory dealing with the coupling of ionic and electronic conduction can and will facilitate breakthroughs in Li-ion battery research.

Acknowledgements

This effort was supported by the General Motors/University of Michigan Advanced Battery Coalition for Drivetrains, with additional sponsorship by the Department of Energy and the Michigan Economic Development Corporation. The authors appreciate the support from our sponsors. We further acknowledge the helpful contributions of Ms. Kelsey Ann Powell and Mr. Conor Douglas Parks in gathering materials for this paper.

References

[1] K. Nakajima, Y. Nishi, in: T. Osaka, M. Datta (Eds.), Advanced Li-ion Batteries. Energy Storage Systems for Electronics, Gordon and Breach Science Publishers, 2000, pp. 109–129.
[2] S. Moore, M. Ehsani, Advances in Electric Vehicle Technology, SAE, SP-1417 1–8 (1999).
[3] V. Srinivasan, J. Newman, Journal of the Electrochemical Society 151 (10) (2004) A1530–A1538.
[4] M. Doyle, J. Newman, Journal of Applied Electrochemistry 27 (1997) 846–856.
[5] C.W. Wang, A.M. Sastry, Journal of the Electrochemical Society 154 (11) (2007), A.1035–1047.
[6] G. Ceder, Y.M. Chiang, D.R. Sadoway, M.K. Aydinol, Y.-I. Jang, B. Huang, Nature 392 (1998) 694–696.
[7] A. Van der Ven, M.K. Aydinol, G. Ceder, G. Kresse, J. Hafner, Physical Review B 58 (6) (1998) 2975–2987.
[8] S. Shi, C. Ouyang, D.S. Wang, L. Chen, X. Huang, Solid State Communications 126 (2003) 531–534.
[9] Y. Makino, T. Kusagaya, K. Suzuki, A. Endou, M. Kubo, P. Selvam, H. Ota, F. Yonekawa, N. Yamazaki, A. Miyamoto, Solid State Ionics 175 (2004) 847–850.
[10] D. Zhang, B.N. Popov, R.E. White, Journal of the Electrochemical Society 147 (3) (2000) 831–838.
[11] X. Zhang, A.M. Sastry, W. Shyy, Journal of the Electrochemical Society 155 (7) (2008) A542–A552.
[12] X. Zhang, W. Shyy, A.M. Sastry, Journal of the Electrochemical Society 154 (10) (2007) A910–A916.
[13] J. Christensen, J. Newman, Journal of Solid State Electrochemistry 10 (2006) 293–319.
[14] Y.-H. Chen, S.D. Bakrania, M.S. Wooldridge, A.M. Sastry, Aerosol Science and Technology 44 (2010) 83–95.
[15] Y.-B. Yi, C.-W. Wang, A.M. Sastry, Journal of the Electrochemical Society 151 (8) (2004) A1292–A1300.
[16] Y.B. Yi, A.M. Sastry, Proceedings of the Royal Society of London Series A-Mathematical Physical and Engineering Sciences 460 (2048) (2004) 2353–2380.
[17] L. Berhan, A.M. Sastry, Journal of Composite Material 37 (8) (2003) 715–740.
[18] L. Berhan, Y.B. Yi, A.M. Sastry, Journal of Applied Physics 95 (9) (2004) 5027–5034.
[19] L. Berhan, Y.B. Yi, A.M. Sastry, E. Munoz, M. Selvidge, R. Baughman, Journal of Applied Physics 95 (8) (2004) 4335–4345.

[20] L. Berhan, A.M. Sastry, Physical Review E 75 (4) (2007) 041120-1–041121-8.
[21] L. Berhan, A.M. Sastry, Physical Review, E 75 (4) (2007) 041121-1–041121-7.
[22] M. Doyle, T.F. Fuller, J. Newman, Journal of the Electrochemical Society 140 (6) (1993) 1526–1533.
[23] T.F. Fuller, M. Doyle, J. Newman, Journal of the Electrochemical Society 141 (1) (1994) 1–10.
[24] P.M. Gomadam, J.W. Weidner, R.A. Dougal, R.E. White, Journal of Power Sources 110 (2) (2002) 267–284.
[25] K. Smith, C.Y. Wang, Journal of Power Sources 161 (1) (2006) 628–639.
[26] Y.H. Chen, C.-W. Wang, X. Zhang, A.M. Sastry, Journal of Power Sources 195 (9) (2010) 2851–2862.
[27] Y.-B. Yi, C. -W. Wang, A.M. Sastry, ASME Journal of Engineering Materials and Technology 128 (1) (2006) 73–80.
[28] Y.-H. Chen, C.-W. Wang, G. Liu, X.-Y. Song, V.S. Battaglia, A.M. Sastry, Journal of the Electrochemical Society 154 (10) (2007) A978–A986.
[29] C.-W. Wang, Y.-B. Yi, A.M. Sastry, J. Shim, K.A. Striebel, Journal of the Electrochemical Society 151 (9) (2004) 1489–1498.
[30] Y. Chen, J.W. Evans, Journal of the Electrochemical Society 143 (9) (1996) 2708–2712.
[31] M. Dubarry, N. Vuillaume, B.Y. Liaw, Journal of Power Sources 186 (2009) 500–507.
[32] G.L. Plett, Journal of Power Sources 161 (2006) 1369–1384.
[33] B.Y. Liaw, X.G. Yang, K. Bethune, Solid Sate Ionics 152–153 (2002) 51–59.
[34] B.Y. Liaw, R.G. Jungst, G. Nagasubramanian, H.L. Case, D.H. Doughty, Journal of Power Sources 140 (2005) 157–161.
[35] H. Huang, S.C. Yin, L.F. Nazar, Electrochemical and Solid-State Letters 4 (10) (2001) A170–A172.
[36] S.Y. Chung, J.T. Bloking, Y.M. Chiang, Nature Materials 1 (2002) 123–128.
[37] P. Heitjans, S. Indris, Journal of Physics: Condensed Matter 15 (2003) R1257–R1289.
[38] J. Molenda, Polish Journal of Chemistry 78 (2004) 1413–1421.
[39] J.-M. Tarascon, M. Armand, Nature 414 (2001) 359–367.
[40] P.G. Bruce, Philosophical Transactions Royal Society of London A 354 (1996) 1577–1594.
[41] D. Linden, Handbook of Batteries, 3rd edition, McGraw-Hill, 2002, pp. 1.3–3.24.
[42] T.L. Brown, H.E. LeMay Jr., B.E. Bursten, Chemistry, 7th edition, Prentice-Hall, 1997, pp. 723–769.
[43] D.R. Gaskell, Introduction to the Thermodynamics of Materials, 3rd edition, Taylor & Francis, 1995, pp.493–542.
[44] M. Winter, R.J. Brodd, Chemical Reviews 104 (2004) 4245–4269.
[45] C. Delacourt, L. Laffont, R. Bouchet, C. Wurm, J.-B. Leriche, M. Morcrette, J.-M. Tarascon, C. Masquelier, Journal of the Electrochemical Society 152 (5) (2005) A913–A921.
[46] M. Kaneko, M. Nakayama, Y. Wakizaka, K. Kanamura, M. Wakihara, Electrochimica Acta 53 (2008) 8196–8202.
[47] D.S. Wilkinson, Mass Transport in Solid and Fluids, Cambridge University Press, 2000.
[48] H. Mehrer, Diffusion in Solids, Springer, 2007, pp. 27–36.
[49] D.A. Porter, K.E. Easterling, Phase Transformations in Metals and Alloys, 2nd edition, Chapman & Hall, 1992, pp. 1–109.
[50] I.G. Currie, Fundamental Mechanics of Fluids, 2nd edition, McGraw-Hill, 1993, p. 261.
[51] E.L. Cussler, Diffusion, Cambridge University Press, 1984.
[52] H. Mehrer, Diffusion in Solids, Springer, 2007, pp. 96–67.
[53] M.E. Glicksman, Diffusion in Solids, John Wiley & Sons, 2000, pp. 343–357.
[54] G.C. Farrington, in: C.A.C. Sequeira, A. Hooper (Eds.), Proceedings of the NATO Advanced Study Institute on Solid State Batteries, Alcabideche, Portugal, September 19-26, 1984.
[55] R.H. Petrucci, W.S. Harwood, General Chemistry, 7th edition, Prentice-Hall, 1997, pp. 315–343.
[56] H. Dehmelt, Physica Scripta T22 (1988) 102–110.
[57] H. Mehrer, Diffusion in Solids, Springer, 2007, pp. 55–67.
[58] H. Mehrer, Diffusion in Solids, Springer, 2007, pp. 127–149.
[59] P.F. Green, Kinetics, Transport, and Structure in Hard and Soft Materials, Taylor & Francis, 2005, pp. 79–121.
[60] P. Atkins, The Elements of Physical Chemistry, 3rd edition, Freeman, 2001.
[61] H. Zabel, S.A. Solin (Eds.), Graphite Intercalation Compound II, Springer-Verlag, 1992.
[62] B. Ammundsen, J. Rozière, M.S. Islam, Journal of Physical Chemistry B 101 (1997) 8156–8163.
[63] B.V. Ratnakumar, S.R. Narayanan, in: M.Z.A. Munshi (Ed.), Handbook of Solid Sate Batteries & Capacitors, World Scientific, 1995, pp. 1–40.
[64] C. Wang, J. Hong, Electrochemical and Solid-State Letters 10 (3) (2007) A65–A69.
[65] D. McLean, Grain Boundaries in Metals, Oxford University Press, 1957.
[66] H.C. Yu, A. Van der Ven, K. Thornton, Applied Physics Letters 93 (2008) 091908-1–091908-3.
[67] J.C. Fisher, Journal of Applied Physics 22 (1) (1951) 74–77.
[68] K.N. Tu, J.W. Mayer, L.C. Feldman, Electronic Thin Film Science for Electrical Engineers and Materials Scientists, McMillan, 1992.
[69] I. Kaur, Y. Mishin, W. Gust, Fundamentals of Grain and Interphase Boundary Diffusion. 3rd, revised and enlarged edition, John Wiley & Sons, LTD, 1995, pp. 1–215.
[70] R.T.P. Wipple, Philosophical Magazine Letters 45 (1954) 1225.
[71] A.D. Le Claire, British Journal of Applied Physics 14 (1963) 351–356.
[72] D.J. Griffiths, Introduction to Quantum Mechanics, 2nd edition, Pearson Education, 2005, pp. 1–40.
[73] S. Datta, Quantum Transport. Cambridge (2005) 33–50.
[74] C. Kittel, Introduction to Solid State Physics, 7th edition, Wiley, 1996, pp. 142–220.
[75] W.D. Callister Jr., Materials Science and Engineering: An Introduction, 4th edition, John Wiley & Sons, 1997, pp. 796–801.
[76] B. Segall, Physical Review 125 (1962) 109–122.
[77] B. Segall, Physical Review 124 (1961) 1797–1806.
[78] K.S. Novoselov, A.K. Geim, S.V. Morozov, D. Jiang, Y. Zhang, S.V. Dubonos, I.V. Grigorieva, A.A. Firsov, Science 306 (2004) 666–669.
[79] B. Partoens, F.M. Peeters, Physical Review B 74 (2006) 075404-1–075404-11.
[80] M. Hess, E. Lebraud, A. Levasseur, Journal of Power Sources 68 (1997) 204–207.
[81] J.P. Kemp, P.A. Cox, Journal of Physics: Condensed Matter 2 (1990) 9653–9667.
[82] S. Shi, C. Ouyang, M. Lei, W. Tang, Journal of Power Sources 171 (2007) 908–912.
[83] J. van Elp, J.L. Wieland, H. Eskes, P. Kuiper, G.A. Sawatzky, Physical Review B 44 (12) (1991) 6090–6103.
[84] K. Ragavendran, A. Nakkiran, P. Kalyani, A. Veluchamy, R. Jagannathan, Chemical Physics Letters 456 (2008) 110–115.
[85] J. Marzec, K. Swierczek, J. Przewoznik, J. Molenda, D.R. Simon, E.M. Kelder, J. Schoonman, Solid State Ionics 146 (2002) 225–237.
[86] J. Molenda, W. Kucza, Solid State Ionics 117 (1999) 41–46.
[87] Y. Liu, T. Fujiwara, H. Yukawa, M. Morinaga, Solar Energy Materials & Solar Cells 62 (2000) 81–87.
[88] Y. Liu, T. Fujiwara, H. Yukawa, M. Morinaga, Solid State Ionics 126 (1999) 209–218.
[89] M.W. Raja, S. Mahanty, R.N. Basu, Journal of Power Sources 192 (2009) 618–626.
[90] Y.J. Wei, X.G. Xu, C.Z. Wang, C. Li, G. Chen, Applied Physics Letters 83 (9) (2003) 1791–1793.
[91] S. Shi, L. Liu, C. Ouyang, D.S. Wang, Z. Wang, L. Chen, X. Huang, Physical Review B 68 (2003) 195108-1–195108-5.
[92] Y.N. Xu, S.Y. Chung, J.T. Bloking, Y.M. Chiang, W.Y. Ching, Electrochemical and Solid-State Letters 7 (6) (2004) A131–A134.
[93] P.R. Wallace, Physical Review 71 (1947) 622–634.
[94] R.E. Hummel, Electronic Properties of Materials, 3rd edition, Springer-Verlag, 2001.
[95] C. Kittel, Introduction to Solid State Physics, 7th edition, Wiley, 1996, pp. 142–172.
[96] J. Ma, C. Wang, S. Wroblewski, Journal of Power Sources 164 (2007) 849–856.
[97] K. Dokko, M. Mohamedi, Y. Fujita, T. Itoh, M. Nishizawa, M. Umeda, I. Uchida, Journal of the Electrochemical Society 148 (5) (2001) A422–A426.
[98] J. Barker, R. Pynenburg, R. Koksbang, M.Y. Saidi, Electrochimica Acta 41 (15) (1996) 2481–2488.
[99] S. Levasseur, M. Ménétrier, C. Delmas, Chemistry of Materials 14 (2002) 3584–3590.
[100] M.Y. Saïdi, J. Barker, R. Koksbang, Journal of Solid State Chemistry 122 (1996) 195–199.
[101] F. Cao, J. Prakash, Electrochimica Acta 47 (2002) 1607–1613.
[102] P.P. Prosini, M. Lisi, D. Zane, M. Pasquali, Solid State Ionics 148 (2002) 45–51.
[103] R.A. Huggins, in: C.A.C. Sequeira, A. Hooper (Eds.), Proceedings of the NATO Advanced Study Institute on Solid State Batteries, Alcabideche, Portugal, September 2–17, 1984.
[104] D. Morgan, A. Van der Ven, G. Ceder, Electrochemical and Solid-State Letters 7 (2) (2004) A30–A32.
[105] C. Ouyang, S. Shi, Z. Wang, X. Huang, L. Chen, Physical Review B 69 (2004) 104303-1–104303-5.
[106] C. Wolverton, A. Zunger, Physical Review B 57 (4) (1998) 2242–2252.
[107] J.B. Goodenough, Solid Sate Ionics 69 (1994) 184–198.
[108] A. Van der Ven, G. Ceder, Electrochemical and Solid-State Letters 3 (7) (2000) 301–304.
[109] Y.I. Jang, B.J. Neudecker, N.J. Dudney, Electrochemical and Solid-State Letters 4 (6) (2001) A74–A77.
[110] M. Okubo, E. Hosono, T. Kudo, H.S. Zhou, I. Honma, Solid State Ionics 180 (2009) 612–615.
[111] J. Xie, N. Imanishi, T. Matsumura, A. Hirano, Y. Takeda, O. Yamamoto, Solid State Ionics 179 (2008) 362–370.
[112] J. Cho, H.S. Jung, Y.C. Park, G.B. Kim, H.S. Lim, Journal of the Electrochemical Society 147 (1) (2000) 15–20.
[113] L.A. Montoro, J.M. Rosolen, Electrochimica Acta 49 (2004) 3243–3249.
[114] S.T. Myung, N. Kumagai, S. Komaba, H.T. Chung, Solid State Ionics 139 (2001) 47–56.
[115] Q. Cao, H.P. Zhang, G.J. Wang, Q. Xia, Y.P. Wu, H.Q. Wu, Electrochemistry Communications 9 (2007) 1228–1232.
[116] H. Wang, W.D. Zhang, L.Y. Zhu, M.C. Chen, Solid State Ionics 178 (2007) 131–136.
[117] K. Dokko, M. Nishizawa, M. Mohamedi, M. Umeda, I. Uchida, J. Akimoto, Y. Takahasi, Y. Gotoh, S. Mizuta, Electrochemical and Solid-State Letters 4 (9) (2001) A151–A153.
[118] S.R. Das, S.B. Majumder, R.S. Katiyar, Journal of Power Sources 139 (2005) 261–268.
[119] D. Singh, W.-S. Kim, V. Craciun, H. Hofmann, R.K. Singh, Applied Surface Science 197–198 (2002) 516–521.
[120] B.J. Johnson, D.H. Doughty, J.A. Voigt, T.J. Boyle, Journal of Power Sources 68 (1997) 634–636.

Please cite this article in press as: M. Park, et al., J. Power Sources (2010), doi:10.1016/j.jpowsour.2010.06.060

[121] A. Veluchamy, H. Ikuta, M. Wakihara, Solid State Ionics 143 (2001) 161–171.
[122] M. Wakihara, L. Guohua, H. Ikuta, T. Uchida, Solid State Ionics 86–88 (1996) 907–909.
[123] H.J. Bang, V.S. Donepudi, J. Prakash, Electrochimica Acta 48 (2002) 443–451.
[124] R. Amin, P. Balaya, J. Maier, Electrochemical and Solid-State Letters 10 (1) (2007) A13–A16.
[125] X.J. Wang, X.Q. Yu, H. Li, X.Q. Yang, J. McBreen, X.J. Huang, Electrochemistry Communications 10 (2008) 1347–1350.
[126] T. Nakamura, K. Sakumoto, M. Okamoto, S. Seki, Y. Kobayashi, T. Takeuchi, M. Tabuchi, Y. Yamada, Journal of Power Sources 174 (2007) 435–441.
[127] R. Amin, C. Lin, J. Maier, Physical Chemistry Chemical Physics 10 (2008) 3524–3529.
[128] H. Liu, Q. Cao, L.J. Fu, C. Li, Y.P. Wu, H.Q. Wu, Electrochemistry Communications 8 (2006) 1553–1557.
[129] S.T. Myung, S. Komaba, No. Hirosaki, H. Yashiro, N. Kumagai, Electrochimica Acta 49 (2004) 4213–4222.
[130] F. Gao, Z. Tang, Electrochimica Acta 53 (2008) 5071–5075.
[131] A. Van der Ven, G. Ceder, Journal of Power Sources 97–98 (2001) 529–531.
[132] Y. Koyama, I. Tanaka, H. Adachi, Y. Uchimoto, M. Wakihara, Journal of the Electrochemical Society 150 (1) (2003) A63–A67.
[133] K. Suzuki, Y. Oumi, S. Takami, M. Kubo, A. Miyamoto, M. Kikuchi, N. Yamazaki, M. Mita, Japanese Journal of Applied Physics 39 (2000) 4318–4322.
[134] A. Van der Ven, G. Ceder, Electrochemical and Solid-State Letters 3 (2000) 301–304.
[135] X. Ouyang, M. Lei, S. Shi, C. Luo, D. Liu, D. Jiang, Z. Ye, M. Lei, Journal of Alloys and Compounds 476 (2009) 462–465.
[136] F. Zhou, M. Cococcioni, C.A. Marianetti, D. Morgan, G. Ceder, Physical Review B 70 (2004), 235121-1–235121-8.
[137] A. Van der Ven, M.K. Aydinol, G. Ceder, Journal of the Electrochemical Society 145 (6) (1998) 2149–2155.
[138] A. Van der Ven, G. Ceder, M. Asta, P.D. Tepesch, Physical Review B 64 (2001), 184307-1–184307-17.
[139] A. Van der Ven, G. Ceder, Electrochemistry Communications 6 (2004) 1045–1050.
[140] R.F. Pierret, Semiconductor Device Fundamentals, Addison-Wesley, 1996.
[141] F.F.C. Bazito, R.M. Torresi, Journal of the Brazilian Chemical Society 17 (4) (2006) 627–642.
[142] D. Aurbach, M.D. Levi, E. Levi, H. Teller, B. Markovsky, G. Salitra, U. Heider, L. Heider, Journal of the Electrochemical Society 145 (9) (1998) 3024–3034.
[143] H.J. Yue, X.K. Huang, D.P. Lv, Y. Yang, Electrochimica Acta 54 (2009) 5363–5367.
[144] R.K. Katiyar, R. Singhal, K. Asmar, R. Valentin, R.S. Katiyar, Journal of Power Sources 194 (2009) 526–530.
[145] D. Shu, K.Y. Chung, W.I. Cho, K.B. Kim, Journal of Power Sources 114 (2003) 253–263.
[146] K.A. Striebel, C.Z. Deng, S.J. Wen, E.J. Cairns, Journal of the Electrochemical Society 143 (1996) 1821–1827.
[147] T. Takamura, K. Endo, J. Fu, Y. Wu, K.J. Lee, T. Matsumoto, Electrochimica Acta 53 (2007) 1055–1061.
[148] J. Xie, N. Imanishi, A. Hirano, M. Matsumura, Y. Takeda, O. Yamamoto, Solid State Ionics 178 (2007) 1218–1224.
[149] L.Q. Chen, W. Yang, Physical Review B 50 (1994) 15752.
[150] J. Park, W. Lu, Physical Review E 80 (2009) 021607.
[151] J. Park, W. Lu, Applied Physics Letters 95 (2009) 073110.
[152] J.E. Guyer, W.J. Boettinger, J.A. Warren, Physical Review E 69 (2004) 021603.
[153] J.E. Guyer, W.J. Boettinger, J.A. Warren, Physical Review E 69 (2004) 021604.
[154] Y. Takahashi, N. Kijima, K. Tokiwa, T. Watanabe, J. Akimoto, Journal of Physics: Condensed Matter 19 (2007), 436202-1–436202-12.
[155] D. Carlier, M. Ménétrier, C. Delmas, Journal of Materials Chemistry 11 (2001) 594–603.
[156] S.M. Lala, L.A. Montoro, V. Lemos, M. Abbate, J.M. Rosolen, Electrochimica Acta 51 (2005) 7–13.
[157] S. Oh, J.K. Lee, D. Byun, W.I. Cho, B.W. Cho, Journal of Power Sources 132 (2004) 249–255.
[158] J.R. Dygas, M. Kopec, F. Krok, D. Lisovytskiy, J. Pielaszek, Solid State Ionics 176 (2005) 2153–2161.
[159] J. Molenda, W. Ojczyk, M. Marzec, J. Marzec, J. Przewoznik, R. Dziembaj, M. Molenda, Solid Sate Ionics 157 (2003) 73–79.
[160] S. Mandal, R.M. Rojas, J.M. Amarilla, P. Calle, N.V. Kosova, V.F. Aunfrienko, J.M. Rojo, Chemistry of Materials 14 (2002) 1598–1605.
[161] J. Molenda, K. Swierczek, J. Marzec, R.S. Liu, Solid State Ionics 157 (2003) 101–108.
[162] M.G. Lazarraga, L. Pascual, H. Gadjov, D. Kovacheva, K. Petrov, J.M. Amarilla, R.M. Rojas, M.A. Martin-Luengo, J.M. Rojo, Journal of Materials Chemistry 14 (2004) 1640–1647.
[163] J. Molenda, J. Marzec, K. Swierczek, W. Ojczyk, M. Ziemnicki, M. Molenda, M. Drozdek, R. Dziembaj, Solid State Ionics 171 (2004) 215–227.
[164] M. Molenda, R. Dziembaj, E. Podstawka, L.M. Proniewicz, Z. Piwowarska, Journal of Power Sources 174 (2007) 613–618.
[165] D.K. Kim, H.M. Park, S.J. Jung, Y.U. Jeong, J.H. Lee, J.J. Kim, Journal of Power Sources 159 (2006) 237–240.
[166] K.F. Hsu, S.Y. Tsay, B.J. Hwang, Journal of Materials Chemistry 14 (2004) 2690–2695.
[167] G.X. Wang, S. Needham, J. Yao, J.Z. Wang, R.S. Liu, H.K. Liu, Journal of Power Sources 159 (2006) 282–286.
[168] C. Delacourt, C. Wurm, L. Laffont, J.-B. Leriche, C. Masquelier, Solid State Ionics 177 (2006) 333–341.
[169] S.L. Bewlay, K. Konstantinov, G.X. Wang, S.X. Dou, H.K. Liu, Materials Letters 58 (2004) 1788–1791.
[170] W. Ojczyk, J. Marzec, K. Swierczek, W. Zajac, M. Molenda, R. Dziembaj, J. Molenda, Journal of Power Sources 173 (2007) 700–706.
[171] H. Kawai, M. Nagata, H. Kageyama, H. Tukamoto, Electrochimica Acta 45 (1999) 315–327.
[172] M. Thackeray, Nature Materials 1 (2002) 81–82.
[173] A. Manthiram, J. Choi, W. Choi, Solid State Ionics 177 (2006) 2629–2634.
[174] E. Antolini, Solid State Ionics 170 (2004) 159–171.
[175] C.A.J. Fisher, V.M. Hart Prieto, M. Saiful Islam, Chemistry of Materials 20 (2008) 5907–5915.
[176] J. Wolfenstine, Journal of Power Sources 158 (2006) 1431–1435.
[177] R. Amin, J. Maier, P. Balaya, D.P. Chen, C.T. Lin, Solid State Ionics 179 (2008) 1683–1687.
[178] Y. Tomita, H. Yonekura, K. Kobayashi, Bulletin of the Chemical Society of Japan 75 (2002) 2253–2256.
[179] A. Yamada, M. Tanaka, Materials Research Bulletin 36 (6) (1995) 715–721.
[180] J.D. Dunitz, L.E. Orgel, Journal of Physics and Chemistry of Solids 3 (1957) 20–29.
[181] F. Nobili, F. Croce, B. Scrosati, R. Marassi, Chemistry of Materials 13 (2001) 1642–1646.
[182] F. Zhou, K. Kang, T. Maxisch, G. Ceder, D. Morgan, Solid State Communications 132 (2004) 181–186.
[183] E. Iguchi, N. Nakamura, A. Aoki, Philosophical Magazine B 78 (1) (1998) 65–77.
[184] K. Zaghib, A. Mauger, J.B. Goodenough, F. Gendron, C.M. Julien, Chemistry of Materials 19 (2007) 3740–3747.
[185] A. Mauger, K. Zaghib, F. Gendron, C.M. Julien, Ionics 14 (2008) 209–214.
[186] L. Wang, Y. Huang, R. Jiang, D. Jia, Journal of the Electrochemical Society 154 (11) (2007) A1015–A1019.
[187] T. Nakamura, Y. Miwa, M. Tabuchi, Y. Yamada, Journal of the Electrochemical Society 153 (6) (2006) A1108–A1114.
[188] C.M. Julien, K. Zaghib, A. Mauger, M. Massot, A. Ait-Salah, M. Selmane, F. Gendron, Journal of Applied Physics 100 (2006), 063511-1–063511-7.
[189] M.M. Doeff, J.D. Wilcox, R. Yu, A. Aumentado, M. Marcinek, R. Kostecki, Journal of Solid State Electrochemistry 12 (2008) 995–1001.
[190] M. Gaberscek, R. Dominko, J. Jamnik, Electrochemistry Communications 9 (2007) 2778–2783.
[191] Mu-Rong Yang, Wei-hsin Ke, Wu. She-huang, Journal of Power Sources 165 (2007) 646–650.
[192] Y.P. Wu, E. Rahm, R. Holze, Journal of Power Sources 114 (2003) 228–236.
[193] M. Noel, V. Suryanarayanan, Journal of Power Sources 111 (2002) 193–209.
[194] J.L. Tirado, Materials Science and Engineering R 40 (2003) 103–136.
[195] L.J. Fu, H. Liu, C. Li, Y.P. Wu, E. Rahm, R. Holze, H.Q. Wu, Solid State Sciences 8 (2006) 113–128.
[196] E. Frackowiak, F. Béguin, Carbon 40 (2002) 1775–1787.
[197] G.M. Ehrlich, in: David Linden (Ed.), Handbook of Batteries, 3rd ed., McGraw-Hill, 2002, pp. 35.16–35.21.
[198] A.V. Churikov, N.A. Gridina, N.V. Churikova, in: V. Igor, Barsukov, S. Christopher, Johnson, E. Joseph, Doninger, Z. Vyacheslav, Barsukov (Eds.), New Carbon Based Materials for Electrochemical Energy Storage Systems, Springer, 2006, pp. 269–276.
[199] M.S. Whittingham, A.J. Jacobson (Eds.), Intercalation Chemistry, Academic Press, 1982.
[200] S.A. Safran, D.R. Hamann, Physical Review Letters 42 (21) (1979) 1410–1413.
[201] M.D. Levi, D. Aurbach, J. Maier, Journal of Electroanalytical Chemistry 624 (2008) 251–261.
[202] H. Zabel, S.A. Solin (Eds.), Graphite Intercalation Compound I, Springer-Verlag, 1990.
[203] J.R. Dahn, Physical Review B 44 (17) (1991) 9170–9177.
[204] M.D. Levi, E. Markevich, D. Aurbach, Electrochimica Acta 51 (2005) 98–110.
[205] S.A. Safran, Physical Review Letters 44 (14) (1980) 937–940.
[206] A. Funabiki, M. Inaba, Z. Ogumi, S.I. Yuasa, J. Otsuji, A. Tasaka, Journal of the Electrochemical Society 145 (1) (1998) 172–178.
[207] Y.N. Li, J. Yang, Z. Jiang, Journal of Physics and Chemistry of Solids 67 (2006) 882–886.
[208] J.K. Lee, K.W. An, J.B. Ju, B.W. Cho, W.I. Cho, D. Park, K.S. Yun, Carbon 39 (2001) 1299–1305.
[209] H. Tachikawa, A. Shimizu, Journal of Physical Chemistry B 110 (2006) 20445–20450.
[210] S.S. Zhang, K. Xu, T.R. Jow, Electrochimica Acta 48 (2002) 241–246.
[211] X.C. Tang, C.Y. Pan, L.P. He, L.Q. Li, Z.Z. Chen, Electrochimica Acta 49 (2004) 3113–3119.
[212] H. Yang, H.J. Bang, J. Prakash, Journal of the Electrochemical Society 151 (8) (2004) A1247–A1250.
[213] Q. Wang, H. Li, X. Huang, L. Chen, Journal of the Electrochemical Society 148 (7) (2001) A737–A741.
[214] M.D. Levi, E. Markevich, D. Aurbach, The Journal of Physical Chemistry B 109 (2005) 7420–7427.
[215] O. Omae, J. Suzuki, T. Katsuta, K. Yamaguchi, F. Kikuchi, K. Sekine, T. Kawamura, T. Takamura, Solid State Ionics 152–153 (2002) 105–110.
[216] J. Suzuki, O. Omae, K. Sekine, T. Takamura, Solid State Ionics 152–153 (2002) 111–118.
[217] T. Uchida, Y. Morikawa, H. Ikuta, M. Wakihara, K. Suzuki, Journal of the Electrochemical Society 143 (8) (1996) 2606–2610.

Please cite this article in press as: M. Park, et al., J. Power Sources (2010), doi:10.1016/j.jpowsour.2010.06.060

[218] N. Takami, A. Satoh, M. Hara, T. Ohsaki, Journal of the Electrochemical Society 142 (2) (1995) 371–379.
[219] M. Nishizawa, H. Koshika, R. Hashitani, T. Itoh, T. Abe, I. Uchida, The Journal of Physical Chemistry B 103 (24) (1999) 4933–4936.
[220] K. Naoi, N. Ogihara, Y. Igarashi, A. Kamakura, Y. Kusachi, K. Utsugi, Journal of the Electrochemical Society 152 (6) (2005) A1047–A1053.
[221] H. Groult, B. Kaplan, S. Komaba, N. Kumagai, V. Gupta, T. Nakajima, B. Simon, Journal of the Electrochemical Society 150 (2) (2003) G67–G75.
[222] M. Endo, Y. Nishimura, T. Takahashi, K. Takeuchi, M.S. Dresselhaus, Journal of Physics and Chemistry of Solids 57 (6–8) (1996) 725–728.
[223] T. Ohzuku, R.J. Brodd, Journal of Power Sources 174 (2007) 449–456.
[224] M. Endo, C. Kim, T. Karaki, T. Tamaki, Y. Nishimura, M.J. Matthews, S.D.M. Brown, M.S. Dresselhaus, Physical Review B 58 (14) (1998) 8991–8996.
[225] U. Tanaka, T. Sogabe, H. Sakagoshi, M. Ito, T. Tojo, Carbon 39 (2001) 931–936.
[226] Q. Wang, H. Li, L. Chen, X. Huang, D. Zhong, E. Wang, Journal of the Electrochemical Society 150 (9) (2003) A1281–A1286.
[227] M.D. Levi, D. Aurbach, Journal of Electroanalytical Chemistry 421 (1997) 79–88.
[228] D.A. Jones, Principles and Prevention of Corrosion, 2nd ed., Prentice Hall, 1997.
[229] V.S. Sastri, Corrosion Inhibitors, Wiley, 1998.
[230] J.R. Davis (Ed.), Corrosion, ASM International, 2000.
[231] D. Bar-Tow, E. Peled, L. Burstein, Journal of the Electrochemical Society 146 (3) (1999) 824–832.
[232] S.S. Zhang, Journal of Power Sources 162 (2006) 1379–1394.
[233] K. Abe, K. Miyoshi, T. Hattori, Y. Ushigoe, H. Yoshitake, Journal of Power Sources 184 (2008) 449–455.
[234] H. Ota, T. Sato, H. Suzuki, T. Usami, Journal of Power Sources 97-98 (2001) 107–113.
[235] D. Aurbach, Y. Ein-Eli, B. Markovsky, A. Zaban, S. Luski, Y. Carmeli, H. Yamin, Journal of the Electrochemical Society 142 (9) (1995) 2882–2890.
[236] E. Peled, D. Golodnitsky, G. Ardel, Journal of the Electrochemical Society 144 (8) (1997) L208–L210.
[237] P.B. Balbuena, Y. Wang (Eds.), Lithium-Ion Batteries, Solid–Electrolyte Interphase, Imperial College Press, 2004.
[238] K. Edstrom, T. Gustafsson, J.O. Thomas, Electrochimica Acta 50 (2004) 397–403.
[239] M. Itagaki, N. Kobari, S. Yotsuda, K. Watanabe, S. Kinoshita, M. Ue, Journal of Power Sources 148 (2005) 78–84.
[240] M. Koltypin, D. Aurbach, L. Nazar, B. Ellis, Electrochemical and Solid-State Letters 10 (2) (2007) A40–A44.
[241] F. Sauvage, L. Laffont, J.-M. Tarascon, E. Baudrin, Journal of Power Sources 175 (2008) 495–501.
[242] T.F. Yi, Y.R. Zhu, X.D. Zhu, J. Shu, C.B. Yue, A.N. Zhou, Ionics 15 (2009) 779–784.
[243] K.A. Walz, C.S. Johnson, J. Genthe, L.C. Stoiber, W.A. Zeltner, M.A. Anderson, M.M. Thackeray, Journal of Power Sources 195 (2010) 4943–4951.
[244] Y. Oh, D. Ahn, S. Nam, B. Park, Journal of Solid State Electrochemistry 14 (2010) 1235–1240.
[245] M.S. Dresselhaus, G. Dresselhaus, Advances in Physics 51 (1) (2002) 1–186.
[246] A.K. Dutta, Physical Review 90 (2) (1953) 187–192.
[247] W.W. Tyler, A.C. Wilson Jr., Thermal Conductivity, Physical Review 89 (4) (1953) 870–875.
[248] S. Bhattacharyya, S.V. Subramanyam, Applied Physics Letters 71 (5) (1997) 632–634.
[249] L. Ravagnan, P. Piseri, M. Bruzzi, S. Miglio, G. Bongiorno, A. Baserga, C.S. Casari, A. Li Bassi, C. Lenardi, Y. Yamaguchi, T. Wakabayashi, C.E. Bottani, P. Milani, Physical Review Letters 98 (2007), 216103-1–216103-4.
[250] P.N. Vishwakarma, S.V. Subramanyam, Journal of Applied Physics 100 (2006), 113702-1–113702-5.
[251] G. Rizzoni, Principles and Applications of Electrical Engineering, 4th ed., McGraw Hill, 2004, pp. 43–44.
[252] K. Kitoh, H. Nemoto, Journal of Power Sources 81–82 (1999) 887–890.
[253] H. Maleki, S.A. Hallaj, J.R. Selman, R.B. Dinwiddie, H. Wang, Journal of the Electrochemical Society 146 (3) (1999) 947–954.
[254] H. Maleki, J.N. Howard, Journal of Power Sources 191 (2009) 568–574.
[255] U.S. Kim, C.B. Shin, C.S. Kim, Journal of the Power Sources 180 (2008) 909–916.
[256] K. Smith, G.H. Kim, E. Darcy, A. Pesaran, International Journal of Energy Research 34 (2010) 204–215.
[257] D.R. Baker, M.W. Verbrugge, Journal of the Electrochemical Society 146 (7) (1999) 2413–2424.
[258] V. Srinivasan, C.Y. Wang, Journal of the Electrochemical Society 150 (1) (2003) A98–A106.
[259] K.E. Thomas, J. Newman, Journal of the Electrochemical Society 150 (2) (2003) A176–A192.
[260] D. Bernardi, E. Pawlikowski, J. Newman, Journal of the Electrochemical Society 132 (1) (1985) 5–12.
[261] R.J. Brodd, W. Huang, J.R. Akridge, Macromolecular Symposia 159 (2000) 229–245.
[262] A. Chagnes, B. Carré, P. Willmann, D. Lemordant, Journal of Power Sources 109 (2002) 203–213.
[263] I. Geoffroy, P. Willmann, K. Mesfar, B. Carré, D. Lemordant, Electrochimica Acta 45 (2000) 2019–2027.
[264] M.S. Ding, T.R. Jow, Journal of the Electrochemical Society 150 (5) (2003) A620–A628.
[265] R.J. Blint, Journal of the Electrochemical Society 142 (3) (1995) 696–702.
[266] K. Hayamizu, Y. Aihara, Electrochimica Acta 49 (2004) 3397–3402.
[267] B. Scrosati, in: J.R. Akridge, M. Balkanski (Eds.), Solid State Microbatteries, Plenum Press, 1990, pp. 103–143.
[268] P.M. Blonsky, D.F. Shriver, P. Austin, H.R. Allcock, Solid State Ionics 18 & 19 (1986) 258–264.
[269] M.C. Smart, B.V. Ratnakumar, S. Surampudi, Journal of the Electrochemical Society 146 (2) (1999) 486–492.
[270] K.M. Abraham, Electrochimica Acta 38 (9) (1993) 1233–1248.
[271] M. Salomon, H.P. Lin, E.J. Plichta, M. Hendrickson, in: W.A. van Schalkwijk, B. Scrosati (Eds.), Temperature Effects on Li-Ion Cell Performance. Advances in Lithium–Ion Batteries, Kluwer Academic/Plenum Publishers, 2002, pp. 309–344.
[272] M.S. Ding, Journal of Chemical & Engineering Data 48 (2003) 519–528.
[273] M.A.B.H. Susan, A. Noda, M. Watanabe, in: Hiroyuki Ohno (Ed.), Electrochemical Aspects of Ionic Liquids, Wiley-Interscience, 2005, pp. 55–74.
[274] K. Xu, Chemical Reviews 104 (2004) 4303–4417.
[275] M. Ue, S. Mori, Journal of the Electrochemical Society 142 (1995) 2577–2581.
[276] M. Schmidta, U. Heidera, A. Kuehnera, R. Oestena, M. Jungnitza, N. Ignat'evb, P. Sartorib, Journal of Power Sources 97/98 (2001) 557–560.
[277] C.W. Walker Jr., J.D. Cox, M. Salomon, Journal of the Electrochemical Society 143 (1996) L80-L82.
[278] S.N. Shkerin, I.A. Profatilova, J.H. Lee, Ionics 15 (2009) 35–42.
[279] C.R. Yang, Y.Y. Wang, C.C. Wan, Journal of Power Sources 72 (1998) 66–70.
[280] P. Ramadass, Bala Haran, Ralph White, N. Branko, Popov, Journal of Power Sources 112 (2002) 606–613.
[281] M.C. Smart, B.V. Ratnakumar, J.F. Whitacre, L.D. Whitcanack, K.B. Chin, M.D. Rodriguez, D. Zhao, S.G. Greenbaum, S. Surampudi, Journal of the Electrochemical Society 152 (2) (2005) A1069–A1104.
[282] R. Premanand, A. Durairajan, B. Haran, R. White, B. Popov, Journal of the Electrochemical Society 149 (1) (2002) A54–A60.
[283] S.S. Zhang, K. Xu, T.R. Jow, Journal of the Electrochemical Society 149 (5) (2002) A586–A590.
[284] M. Ribes, in: R. James, Akridge, Minko Balkanski (Eds.), Solid State Microbatteries, Plenum Press, 1990, pp. 41–58.
[285] M. Wakihara, Materials Science and Engineering R 33 (2001) 109–134.
[286] K. Zaghib, P. Charest, A. Guerfi, J. Shim, M. Perrier, K. Striebel, Journal of Power Sources 134 (2004) 124–129.
[287] C.Y. Chiang, Y.J. Shen, M. Jaipal Reddy, P. Peter, Chu., Journal of Power Sources 123 (2003) 222–229.
[288] M. Kaneko, M. Nakayama, M. Wakihara, Journal of Solid State Electrochemistry 11 (2007) 1071-1076.
[289] M. Egashira, H. Todo, N. Yosimoto, M. Morita, Journal of Power Sources 178 (2008) 729–735.
[290] S. Zhang, Y. Jim, L. Lee, Hong, Journal of Power Sources 134 (2004) 95–102.
[291] A. Abouimrane, P.S. Whitfield, S. Niketic, I.J. Davidson, Journal of Power Sources 174 (2007) 883–888.
[292] K.Y. Yang, K.Z. Fung, I.C. Leu, Journal of Alloys and Compounds 438 (2007) 207–216.
[293] T. Savitha, S. Selvasekarapandian, C.S. Ramya, M.S. Bhuvaneswari, G. Hirankumar, R. Baskaran, P.C. Angelo, Journal of Power Sources 157 (2006) 533–536.
[294] R. Kanno, T. Hata, Y. Kawamoto, M. Irie, Solid State Ionics 130 (2000) 97–104.
[295] Y. Tomita, H. Matsushita, K. Kobayashi, Y. Maeda, K. Yamada, Solid State Ionics 179 (2008) 867–870.
[296] V. Thangadurai, J. Schwenzel, W. Weppner, Ionics 11 (2005) 11–23.
[297] Y. Hamon, A. Douard, F. Sabary, C. Marcel, P. Vinatier, B. Pecquenard, A. Levasseur, Solid State Ionics 177 (2006) 257–261.
[298] J.H. Kennedy, Z. Zhang, Journal of the Electrochemical Society 135 (4) (1988) 859–862.
[299] T. Inada, K. i Takada, A. Kajiyama, M. Kouguchi, H. Sasaki, S. Kondo, M. Watanabe, M. Murayama, R. Kanno, Solid State Ionics 158 (2003) 275–280.
[300] B.V.R. Chowdari, G.V. Subba Rao, G.Y.H. Lee, Solid State Ionics 136–137 (2000) 1067–1075.
[301] Y. Seino, K. Takada, B.C. Kim, L. Zhang, N. Ohta, H. Wada, M. Osada, T. Sasaki, Solid State Ionics 176 (2005) 2389–2393.
[302] M.A. Ratner, D.F. Shriver, Chemical Reviews 88 (1988) 109–124.
[303] B.L. Papke, M.A. Ratner, D.F. Shriver, Journal of the Electrochemical Society 129 (8) (1982) 1694–1701.
[304] Polymer Handbook, 4th ed., in: J. Brandup, E.H. Immergut, E.A. Grulke (Eds.), A. Abe, D.R. Bloch (Associate Editors), John Wiley and Sons, 1999.
[305] J.F. Le Nest, S. Callens, A. Gandini, M. Armand, Electrochimica Acta 37 (9) (1992) 1585–1588.
[306] A. Nishimoto, M. Watanabe, Y. Ikeda, S. Kohjiya, Electrochimica Acta 43 (1998) 1177–1184.
[307] Bruno, Scrosati, in: A. Walter, van Schalkwijk, Bruno Scrosati (Eds.), Advances in Lithium–Ion Batteries, Kluwer Academic/Plenum Publishers, 2002, pp. 252–266.
[308] C. Svanberg, J. Adebahr, R. Bergman, L. Börjesson, B. Scrosati, P. Jacobsson, Solid State Ionics 136–137 (2000) 1147–1152.
[309] M.J.G. Jak, F.G.B. Ooms, E.M. Kelder, W.J. Legerstee, J. Schoonman, A. Weisenburger, Journal of Power Sources 80 (1999) 83–89.
[310] J.-M. Tarascon, A.S. Gozdz, C. Schmutz, F. Shokoohi, P.C. Warren, Solid State Ionics 86–88 (1996) 49–54.
[311] H. Ohno, in: H. Ohno (Ed.), Electrochemical Aspects of Ionic Liquids, Wiley-Interscience, 2005, pp. 1–3.
[312] A. Webber, G.E. Blomgren, in: W. van Schalkwijk, B. Scrosati (Eds.), Advances in Lithium-Ion Batteries, Kluwer Academic/Plenum Publishers, 2002, pp. 185–232.

Please cite this article in press as: M. Park, et al., J. Power Sources (2010), doi:10.1016/j.jpowsour.2010.06.060

[313] J.S. Lee, J.Y. Bae, H. Lee, N.D. Quan, H.S. Kim, H. Kim, Journal of Industrial and Engineering Chemistry 10 (7) (2004) 1086–1089.
[314] M. Ishikawa, T. Sugimoto, M. Kikuta, E. Ishiko, M. Kono, Journal of Power Sources 162 (2006) 658–662.
[315] H. Matsumoto, H. Sakaebe, K. Tatsumi, Journal of Power Sources 146 (2005) 45–50.
[316] T. Sato, T. Maruo, S. Marukane, K. Takagi, Journal of Power Sources 138 (2004) 253–261.
[317] C.A. Angell, W. Xu, M. Yoshizawa, A. Hayashi, J.-P. Belieres, P. Lucas, M. Videa, in: H. Ohno (Ed.), Electrochemical Aspects of Ionic Liquids, Wiley-Interscience, 2005, pp. 5–23.
[318] Y. Umebayashi, T.I. Mitsugi, S. Fukuda, T. Fujimori, K. Fujii, R. Kanzaki, M. Takeuchi, S.I. Ishiguro, Journal of Physical Chemistry B 111 (2007) 13028–13032.
[319] H. Nakagawa, S. Izuchi, K. Kuwana, T. Nukuda, Y. Aihara, Journal of the Electrochemical Society 150 (6) (2003) A695–A700.
[320] H. Sakaebe, H. Matsumoto, K. Tatsumi, Electrochimica Acta 53 (2007) 1048–1054.
[321] M. Holzapfel, C. Jost, P. Novák, Chemical Communications (2004) 2098–2099.
[322] Y. Gu, D. Cheng, X. Jiao, Journal of Physical Chemistry B 109 (2005) 17901–17906.
[323] Y. Gu, D. Chen, X. Jiao, F. Liu, Journal of Materials Chemistry 17 (2007) 1769–1776.
[324] C.K. Chan, X.F. Zhang, Y. Cui, Nano Letters 8 (1) (2008) 307–309.
[325] L.F. Cui, R. Ruffo, C.K. Chan, H. Peng, Y. Cui, Nano Letters 9 (1) (2009) 491–495.
[326] M.S. Bhuvaneswari, N.N. Bramnik, D. Ensling, H. Ehrenberg, W. Jaegermann, Journal of Power Sources 180 (2008) 553–560.
[327] R. Ruffo, S.S. Hong, C.K. Chan, R.A. Huggins, Y. Cui, Journal of Physical Chemistry C 113 (2009) 11390–11398.
[328] H. Wolf, Z. Pajkic, T. Gerdes, M. Willert-Porada, Journal of Power Sources 190 (2009) 157–161.

Please cite this article in press as: M. Park, et al., J. Power Sources (2010), doi:10.1016/j.jpowsour.2010.06.060